FINITE ELEMENT ANALYSIS OF INDENTATION IN FIBER-REINFORCED POLYMER COMPOSITES

A Thesis

by

ARUN RAVISHANKAR

Submitted to the Office of Graduate Studies of
Texas A&M University
in partial fulfillment of the requirements for the degree of

MASTER OF SCIENCE

May 2011

Major Subject: Mechanical Engineering

FINITE ELEMENT ANALYSIS OF INDENTATION IN FIBER-REINFORCED POLYMER COMPOSITES

A Thesis

by

ARUN RAVISHANKAR

Submitted to the Office of Graduate Studies of
Texas A&M University
in partial fulfillment of the requirements for the degree of

MASTER OF SCIENCE

Approved by:

Co-Chairs of Committee,	Anastasia Muliana
	K. R. Rajagopal
Committee Members,	James E. Moore, Jr.
Head of Department,	Dennis O'Neal

May 2011

Major Subject: Mechanical Engineering

ABSTRACT

Finite Element Analysis of Indentation in Fiber-Reinforced Polymer Composites.

(May 2011)

Arun Ravishankar, B.E., B.M. Sreenivasaiah College of Engineering, Bangalore

Co–Chairs of Advisory Committee: Dr. Anastasia Muliana
Dr. K. R. Rajagopal

This thesis employs a finite element (FE) method for numerically simulating the mechanical response of constituents in a fiber-reinforced polymer (FRP) composite to indentation. Indentation refers to a procedure that subsumes a rigid indenter of specific geometry to impress the surface of a relatively softer material, with a view of estimating its mechanical properties. FE analyses are performed on a two-dimensional simplified microstructure of the FRP composite comprising perfectly bonded fiber, interphase and matrix sections. Indentation response of the constituents is first examined within the context of linearized elasticity. Time-dependent response of the polymer matrix is invoked by modeling the respective constituent section as a linear isotropic viscoelastic material. Furthermore, indentation responses to non-mechanical stimulus, like moisture absorption, is also simulated through a sequentially coupled analysis. A linear relationship describing the degradation of elastic moduli of the individual constituents with increasing moisture content has been assumed. The simulations subsume a point load idealization for the indentation load eventually substituted by indenter tips with conical and spherical profiles. Results from FE analyses in the form of load-displacement curves, displacement contours and stress contours are presented and discussed.

With the application of concentrated load on linearly elastic constituents for a given/known degree of heterogenity in the FRP, simulations indicated the potential of indentation technique for determining interphase properties in addition to estimating the matrix-fiber interphase bond strength. Even with stiffer surrounding constituents, matrix characterization was rendered difficult. However, fiber properties were found to be determinable using the FE load-displacement data, when the load-displacement data from experimentation is made available. In the presence of a polymer (viscoelastic) matrix, the surrounding elastic constituents could be characterized for faster loading rates when viscoelastic effects are insignificant. Displacements were found to be greater in the presence of a polymer matrix and moisture content in comparison with a linearly elastic matrix and dry state. As one would expect, the use of different indenter tips resulted in varying responses. Conical tips resulted in greater displacements while concentrated load produced greater stresses.

Further it was found that, despite the insignificant effects due to surrounding constituents, analytical (*Flamant*) solution for concentrated, normal force on a homogeneous, elastic half-plane becomes inapplicable in back calculating the elastic moduli of individual FRP constituents. This can be attributed to the finite domain and the associated boundary conditions in the problem of interest.

To *my parents and all my teachers whom I always revere*

ACKNOWLEDGMENTS

My sincere thanks to Dr. Muliana for her time and patience in constantly guiding me through the research. I am grateful to Dr. Rajagopal for providing me with an unique opportunity to pursue mechanics under his tutelage, as well as his timely advice and encouragement. I convey my regards to Dr. Moore for obliging to be my committee member. I wish to thank the Texas A&M Mechanical Engineering Department for the award of a fellowship (2009-2010) and the Texas A&M supercomputing facility for providing the necessary resources. The timely assistance with ABAQUS, provided by my friends Mr. Pradeep Gudlur and Mr. Ajay Shastri, is also greatly acknowledged. A special thanks to my friends, Mr. Abhineeth Akkasale and Mr. Rohit Saha, for their insightful comments and suggestions. The least I can do is to mention that I will always be indebted to my parents. Lastly, my regards to all those who have been supportive in any respect.

The financial support provided by NSF-CMMI - National Science Foundation, Division of Civil, Mechanical and Manufacturing Innovation under Grant # 0546528 is also gratefully acknowledged.

TABLE OF CONTENTS

LIST OF TABLES

TABLE Page

LIST OF FIGURES

FIGURE Page

FIGURE Page

CHAPTER I

INTRODUCTION

Load and depth sensing indentation is widely recognized as a reliable tool for evaluating the mechanical properties of a diverse spectrum of materials with reasonable accuracy [1]. Indentation testing is viewed to be advantageous over the traditional uniaxial tests since it is capable of characterizing localized material properties beneficial for small samples. A typical indentation process is characterized by a stiff indenter, when compared to the stiffness of the substrate, penetrating normally into the material of interest at a constant load-displacement rate until a certain load or depth is reached. Load on the indenter is then gradually removed while displacement is recorded continuously during one complete cycle of loading and unloading [2, 3].

Though numerous efforts have been made to gather load-displacement data and consequently estimate the material properties through experimentation, there is yet a considerable lack of understanding of the deformation due to indentation involving areas of the order of micrometers, such as interphase [1] regions in heterogeneous materials [4]. Due to increasing use of small mechanical structures, functionally graded materials and other heterogeneous materials in various engineering applications as in electronics, mechanical and biomedical engineering, critical evaluation of stresses and deformations constitute a prime aspect of the indentation analysis [5]. Recent developments in micro-nano indentation have proven the ability of this technique to characterize mechanical properties of materials at micron and sub-micron length

---

The journal model is *IEEE Transactions on Automatic Control*.

[1]The term *Interface* corresponds to the boundary or plane of contact between the adhesive and the matrix/fiber sections, while *Interphase* refers to the region containing the interfaces when there is a thickness associated with this adhesive layer.

scales, thus allowing individual constituents and local regions of heterogeneous materials to be characterized individually [6]. This is particularly important for understanding the mechanical response of heterogeneous materials in general, for e.g., polymer composite materials or even biological materials in which localized material structure can significantly impact the overall or bulk behaviour [6]. A shortcoming of the technique however, is the resulting boundary value problem that renders the analyses formidable [7].

Environmental effects such as heat conduction and(or) moisture absorption in a material will have a profound influence on its properties. For example, even small quantities of moisture absorbed from the environment can significantly affect the mechanical and physical properties of polymer composites and therefore need to be factored in the characterization of materials [8]. Therefore, it would be intriguing to include the effect of moisture diffusion while simultaneously indenting the material. Consequently, the added complexity to the displacement field precludes a closed-form solution, since coupled deformation-diffusion processes, stress concentration effects, viscoelasticity and contact are all involved. Thus, a numerical technique such as finite element (FE) method is employed for obtaining a solution to the coupled problem.

Indentation problems have received extensive investigations by many researchers till date. They chiefly comprise analytical, experimental and numerical aspects involving a wide range of materials and indenter geometries. The following paragraphs selectively list the relevant literature besides furnishing the course of research.

A. Indentation: A review

Amongst many problems studied, the solution provided by Hertz in 1881 for stresses resulting due to contact between two elastic bodies whose mechanical responses are

isotropic [9] and the analytical solution to axisymmetric Boussinesq problem for a punch of arbitrary profile derived by Sneddon [10] are of mathematical relevance, since indentation involves contact as well as deformation under normal loading.

Giannakopoulos and Suresh [11] derived analytical solutions to the problem of an inhomogeneous, linearly elastic semi-infinite solid surface indented by a point load, for variation of Young's modulus and different fixed values of Poisson's ratio. Young's modulus was varied as a function of the depth below the indented surface, accounting for the elastic inhomogeneity. The quasistatic analysis assumed small deformations and locally isotropic material response. Stresses and displacements were also computed by running FE simulations using a subroutine compatible with ABAQUS. In a sequel to the aforementioned work, the authors [11] presented analytical results for indentation by rigid, frictionless indentors of circular, spherical and conical profiles instead of a point load. FE results were compared with their analytical counterparts for validation.

Laursen and Simo [12] investigated the microindentation of aluminium and silicon in their bulk forms and thin-film substrate combinations by rigid conical indenter, through a FE code called FEAP. A hyperelastic constitutive model based on multiplicative decomposition of the deformation gradient into elastic and plastic components described the indented material behaviour. During unloading, FE simulations indicated changes in contact area which contradicts the popular assumption of a constant area of contact.

Taljat et al. [13] analyzed ball indentation process in metal alloys using ABAQUS FE code. The FE technique subsumed a deformable indenter and an elasto-plastic constitutive law for isotropic materials. Sadeghipour et al. [14] studied elastic and elastic-plastic responses of spherical micro-indentation in polymer-based brittle materials, using FEM. The study focused more on large deformations, distribution of

stresses and strains for edifying the crack phenomena and disregarded viscoelastic effects. ANSYS and ADINA were used in their study. FE technique describing the elastic-plastic response of a flat specimen due to spherical indentation stress fields, with practical relevance to deformation in ceramic materials was developed by Care et al. [15]. They employed specialized gap elements of considerably larger stiffness, preventing an intrusive contact between the indenter and the specimen. Mesarovic and Fleck [16] report their FE study of normal indentation in an elastic-plastic half-space by a rigid sphere. Frictional effects between the surfaces of indenter and specimen were also investigated. FE analysis of indentation of a homogeneous half-space by a rigid spherical indenter was carried out by Kral et al. [17]. The simulations were based on an elastic-plastic constitutive model and were run on ABAQUS.

Mechanical response of heterogeneous materials is also studied through the technique of indentation. Clayton and co-workers [18] identified the inadequacy of their simulations to describe spherical indentation response of metal-polymer composites. Homogeneous elastic-perfectly plastic behaviour assumed for the simulation of these materials failed to capture viscoelastic response induced by polymer component in the microstructure. Shen and Guo [19] concluded that heterogeneous materials cannot be regarded as homogenized materials for indentation modeling. The conclusion was reached after conducting FE analysis on a soft, elastic-plastic matrix section with harder, embedded elastic particles and its homogenized counterpart, with the same overall stress-strain responses.

Substantial portion of indentation tests are attributed to mechanical property determination, while some are associated with interpretation of load-displacement curves and(or) factors affecting the indentation process. Indentation technique is useful in characterizing mechanical properties of thin films. Gan and Ben-Nissan [20] performed FE analysis of thin films to understand the relationship between the

indentation curves and film material properties, for spherical indenters of different radii. Knapp et al. [21] developed a model based on FE method for extraction of material properties of thin films for which coventional analytical treatments fail. However, its inability to model time dependent behaviour such as creep was reported.

Applicability of indentation tests for the mechanical characterization of composite materials is also noteworthy. Zidi et al. [22] conducted Vickers indentation tests on the fiber of a unidirectional glass/epoxy composite for the strength assessment of its matrix-fiber interphase. Their study rested on the assumption that the measured displacement comprises surface indentation and compression components. The latter component associated with intefacial behaviour was extracted from experiments by means of an analytical model incorporating matrix-fiber debonding and fiber sliding. The model was further validated by FE simulations. A detailed study for characterizing the interphase properties by indentation in fiber-reinforced polymer (FRP) composites was undertaken by Desaeger and Verpoest [23]. Shear-lag[2] theory formed the basis for calculating the interfacial shear strength from experiments. In their nonlinear FE parametric study of microindentation in carbon fiber/epoxy composite, Ho and Drzal [24] observed that, the ratio of interfacial shear stress to fiber axial stress is nearly a constant for different fiber diameters. They recorded marginal changes in the interfacial shear stress and indenter displacement with increasing interphase modulus and interphase thickness, for a given fiber diameter. Load on the indenter increased with fiber diameter causing a corresponding increase in the indenter displacement so that interfacial shear strength to axial fiber stress ratio is nearly a constant. This explains the difference in slopes of the load-displacement curves which are insensitive to interphase properties. Hence, indentation curves cannot be directly used to char-

[2]A delay or slow response in developing shear flow reactions to applied loads (©1989 CRC Press LLC.).

acterize interphase properties. FE results were found to be in agreement with the shear-lag analysis and an empirical derivation, for a certain range of the fiber volume fraction.

Larsson and Carlsson [7] derived rigorous relations to completely characterize viscoelastic polymers by indentation besides citing the exhaustive theoretical framework at disposal, necessary for characterizing such materials by spherical and cylindrical indenters. Lu et al. [5] demonstrated the pertinence of indentation load-displacement data to determine the creep compliance of time-dependent materials. They conducted experiments on solid polymers for computing the creep compliance functions of linearly viscoelastic materials subjected to Berkovich and spherical indention. Indentation test data was further verified with that from traditional tension and shear tests on the polymers. Odegard et al. [6] determined the dynamic viscoelastic properties of polymeric materials through indentation and obtained consistent results from the dynamic mechanical analysis. Sakai [25], using principle of superposition, obtained the viscoelastic solution to the axisymmetric flat-ended, spherical and conical indenter problems by modifying the solution for that of an elastic contact. Time-dependent load-depth relations were arrived at, after conducting numerical analyses on simple viscoelastic solid-like and fluid-like models. Storåkers and Larsson [26] developed a theoretical framework for indentation analyses of creeping solids as opposed to the uniaxial tests based on a power law constitutive relation for creep. Inelastic response of materials were investigated and a FE procedure incorporating mixed variational principle was used for accuracy of results. Boussinesq creep test involving a flat cylindrical indenter was viewed advantageous over that using a spherical indenter.

Kumar and Narasimhan [27], in their study of spherical indentation of linear viscoelastic materials, testified the accuracy of depth-sensing indentation technique for characterizing the mechanical response of linear isotropic viscoelastic materials

through comparison with conventional mechanical test data. They also compared the analytical solution with experiments and FE analysis performed on polymethyl methacrylate.

Several studies on determining responses of biomaterials using indentation technique have been presented. Carrillo et al. [28] attempted to validate the credibility of nano-indentation technique to describe the mechanical response of softer (elastic modulus below 5 MPa) biological materials, incorporating the assumptions of classical linearized elasticity. Recently, Gupta et al. [29] verified the ability of depth sensing indentation for accurately determining properties of biomaterials which exhibit non-linear viscoelastic behavior. Their assessments were based on a model (fibril reinforced poroviscoelastic) used to simulate indentation process in porcine costal cartilage.

B. Motivation and course of research

Recent indentation studies have extensively focused on understanding the elastic and plastic responses of homogeneous materials in addition to evaluating mechanical properties. Limited studies have shown the capability of indentation tests to characterize bond strength and constituent properties of composite (heterogeneous) materials. Understanding the mechanical response of heterogeneous materials with viscoelastic constituents using indentation technique is far from satisfactory. Thus, there is a need for further investigation. Furthermore, it is understood that localized response of a constituent in heterogeneous materials depend upon properties of its surrounding constituents. This can place difficulties in characterizing properties of a constituent from an indentation response, since it is not always possible to know a priori, the properties/behaviour of all other constituents. Also, the mechanical response during

indentation will be affected in the presence of moisture.

The present work aims to examine the mechanical response of constituents (matrix, interphase and fiber) of a FRP composite during indentation process. ABAQUS, a commercially available FE analysis package is used for the simulations. Load-displacement data are extracted for indentation at the center of fiber, interphase and matrix regions separately for varying stiffness ratios (in the case of elastic constituents) and different loading rates (considering effects of concentration and viscoelasticity). Further, significance of results is discussed with respect to the load-displacement curves and contour plots for typical loading scenarios.

As a first step, plane strain deformation problem is considered in Chapter II. The indentation load is idealized as a point load. The individual constituents (matrix, interphase and fiber) of the composite material are modelled as homogeneous, linearly elastic solids whose mechanical responses are assumed to be isotropic. Response to a concentrated load applied at the mid-points of each constituent section is seeked within a FE setting. A parametric study based on stiffness ratios of individual constituents is carried out while each constituent is indented. The nodal displacement is recorded for loading and unloading times. Indentation load-displacement curves so obtained, are interpreted. Further, a sequentially coupled moisture diffusion-deformation analysis is performed on the rectangular domain considered a priori. FE solution to a transient mass diffusion problem with appropriate boundary conditions is obtained. The nodal concentrations are given as input to the indentation problem, where the material moduli of individual constituents are allowed to degrade with increasing moisture concentration. Effect of moisture concentration on loading and unloading indentation curves are discussed.

The matrix material being a polymer, exhibits viscoelastic behaviour. These effects are studied in Chapter III with the matrix being modelled as a viscoelastic solid-

like material. Load-displacement curves from indentation are extracted for different rates and locations of loading. FE solution for the coupled diffusion-deformation problem is also obtained. Constitutive relations for the polymer matrix are modified based on a time-temperature superposition principle, consequently varying the creep compliance as a function of moisture concentration. As opposed to the mere idealization of indentation by a point load, detailed indenter tip profiles (spherical and conical) are incorporated to study their influence on the loading-unloading curves.

Summary of results with conclusions are presented in Chapter IV.

CHAPTER II

INDENTATION RESPONSE OF LINEARLY ELASTIC CONSTITUENTS

Indentation response of the constituents namely, matrix, interphase and fiber in a FRP composite is examined within the realm of linearized elasticity. As indentation technique is often used to characterize properties of constituents in heterogeneous materials, it is important to understand localized responses while indenting each constituent and the effects of its surrounding constituents on the localized responses during the indentation process.

Indentation is done by pushing or pressing the materials with an indenter that is relatively small in size with respect to the medium being indented. Various nano-micrometer sized indenters of spherical, conical, pyramidal and cylindrical shapes are used. The size and shape of indenters will certainly affect the measured localized response. In addition, material characteristic, which in this particular study is determined by the elastic stiffness of the linearly elastic constituents, significantly influences the indentation response. In this chapter, an idealized problem of indentation on linearly elastic FRP matrix composite is presented. The purpose is to examine the effects of elastic stiffness of each constituent on the localized response during indentation in the fiber, matrix and interphase regions. The following assumptions are made: A two-dimensional representative microstructure of the FRP composite with 45% fiber volume content is considered, as shown in Figure 2.1. A concentrated force is applied to simulate the indentation. Indentation is performed at the center of the fiber, interphase and matrix regions separately. The three constituents are assumed isotropic, linear elastic with respect to their mechanical response. It is noted that fiber properties are usually not isotropic (but transversely isotropic); in order to understand the effect of stiffness on fibers with clarity, its response is considered to be

isotropic. The indentation is effectuated by application of a concentrated force (per unit thickness of the section) of magnitude P $(= 1\ N)$ on each constituent in the micro-section of the composite. While the elastic moduli of fiber (E_f) and interphase (E_i) are expressed in terms of the Young's modulus of matrix (E_m), the Poisson's ratio (ν) is held constant $(= 0.2)$ for all the constituents.

The first part of this chapter presents parametric studies on effects of elastic stiffness of the constituents, for example, indenting a softer constituent with stiffer surrounding constituents and indenting a stiffer constituent with softer surrounding constituents. The second part of this chapter focuses on the effect of non-mechanical stimulus such as moisture diffusion on the indentation response.

A. Problem description and modeling

ABAQUS, a commerical FE package is employed for the analysis, since it supports a vast library of elements and list of constitutive models available for analyses of problems across different domains with varying complexities in geometry and material behaviour. It also supports UMAT, a subroutine for user-defined constitutive modeling. Most of the FE packages including ABAQUS has no system of units built into it and stipulates that all input data be consistent with regard to their units. This is of prime importance if one seeks results with meaningful physical interpretations. Hence, true values for load, geometric dimensions and material moduli are used to enforce the aforesaid consistency. Mesh convergence study has been done and discussed in Appendix A. This is undertaken to determine the mesh size required for accuracy in solution, thus ensuring that the results are not affected by change of mesh size. However, if one prefers to work with dimensionless variables, non-dimensionalization can be carried out in the following manner. Use will be made of *Flamant* solution for

displacement $v(x, y)$ mentioned in Appendix A, the functional form for which reads:

$$v = f(P, E, x, y) \ , \tag{2.1}$$

where v, x, y and P, E are respectively the variables and parameters involving dimensions. Setting

$$\bar{v} := \frac{v}{L}; \quad \bar{x} = \frac{x}{L}; \quad \bar{y} = \frac{y}{L}; \quad \bar{E} = \frac{E}{E_o}; \quad \bar{P} = \frac{P}{E_o L},$$

with L as characteristic length and E_o as reference material modulus, Equation (2.1) in the non-dimensional form can be written as:

$$\bar{v} = g(\bar{P}, \bar{E}, \bar{x}, \bar{y}). \tag{2.2}$$

The actual displacement can then be calculated by multiplying the non-dimensional displacement $\bar{v}$ with L.

A rectangular cross-section of the composite ($1.0\ mm \times 0.5\ mm$) containing fiber, interphase and matrix constituents, forms the domain of interest for FE analysis (Figure 2.1). The volume fractions of fiber (V_f), interphase (V_i) and matrix (V_m) are respectively 0.45, 0.10 and 0.45. E_m is chosen to be 1000 MPa, since the matrix stiffness is typically of the order of GPa. Figure 2.2 illustrates the plausible displacement boundary conditions that could be imposed on the geometry, for indentation loading.

Fiber is considered to be stiffer than the matrix which is generally true of FRP composites. It is assumed that perfect bonding exists between individual constituents within the composite material. In the sequentially coupled diffusion-deformation analysis, concentration boundary condition is applied on the top surface of the geometry, accounting for moisture diffusion. The diffusivities of matrix (D_m), interphase (D_i)

and fiber (D_f) are chosen to be in the ratio $10 : 5 : 1$.

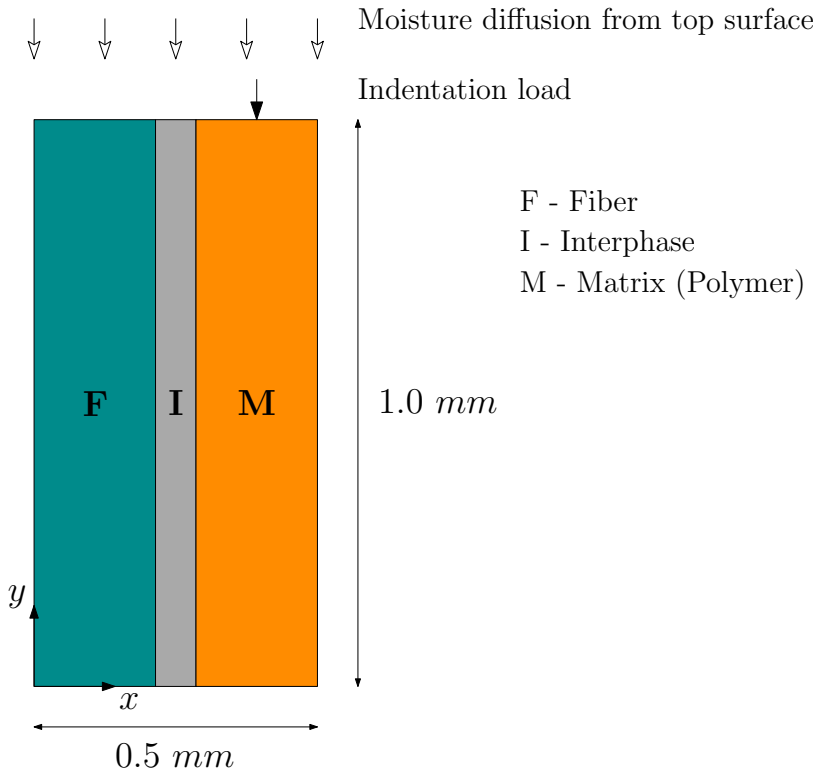

Figure 2.1. Geometry for the finite element analysis.

The geometry is meshed using four noded, quadrilateral elements, CPE4 (plane strain) and DC2D4 (mass diffusion), for deformation and diffusion problems respectively. By default, plane strain thickness is set to unity. A finer mesh size is adopted in the immediate neighbourhood of the loading location to precisely capture the associated displacement gradients. Regions away from the points of loading can work with a relatively coarser mesh size without a trade-off between accuracy of results and cost-effective computations. The FE mesh generated in ABAQUS with 21238

nodes and 21003 elements is as illustrated by Figure 2.3.

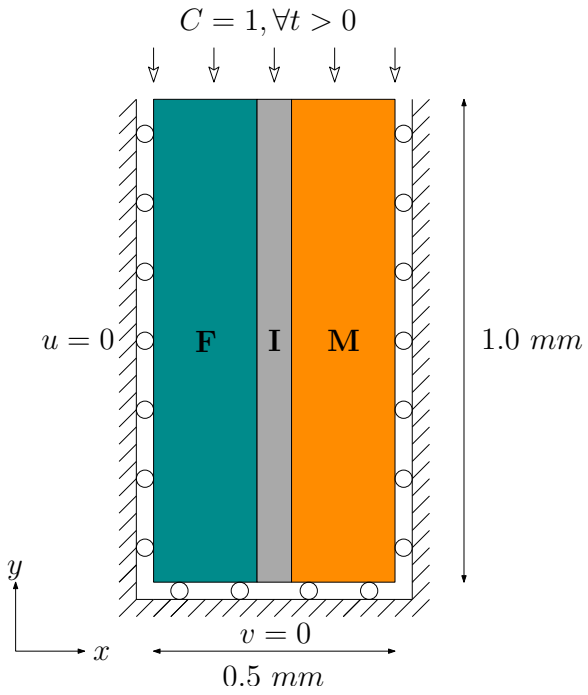

Figure 2.2. Boundary conditions.

B. Deformation problem

In this analysis, matrix, interphase and fiber sections are indented, one at a time. This is achieved by application of a concentrated load at the node corresponding to the midpoint of each constituent section. This choice of loading location entails fairly accurate characterization of mechanical properties of the constituent being indented. Locations other than midsections are influenced by the response of surrounding constituents and hence will not result in the true evaluation of mechanical properties. Different responses will be obtained for different loading locations. The loading is quasistatic and applied as a ramp until a magnitude of unity is reached in a certain time interval. This is followed by removal of load at the same rate as that of loading.

The displacement field $\mathbf{u} = u(x, y)\mathbf{i} + v(x, y)\mathbf{j}$, for a plane strain problem with respect to the x-y plane, due to loading is determined by solving the governing equations for elasto-statics in ABAQUS[3]:

$$div\mathbf{T} + \rho\mathbf{b} = 0. \tag{2.3}$$

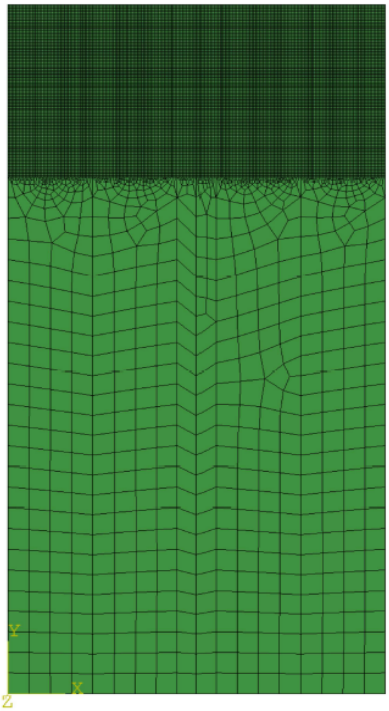

Figure 2.3. Finite element mesh.

Equation (2.3) is a consequence of the balance of linear momentum where ρ is the density, $\mathbf{b}$ is the specific body force. The Cauchy stress tensor for a linearized elastic solid,

$$\mathbf{T} = \lambda(tr\boldsymbol{\varepsilon})\mathbf{I} + 2\mu\boldsymbol{\varepsilon}. \tag{2.4}$$

[3]One may refer to the ABAQUS theory manual [30] for details on the FE formulation and implemention.

λ and μ are Lamé constants and $\mathbf{I}$ is the identity tensor. In the absence of internal couples, the balance of angular momentum will imply that $\mathbf{T} = \mathbf{T}^T$. The linearized strain,

$$\boldsymbol{\varepsilon} = \frac{1}{2}[(\nabla \mathbf{u}) + (\nabla \mathbf{u})^T]. \tag{2.5}$$

Here, displacement boundary conditions are prescribed along the three segments of the boundary (Figure 2.2) while the concentrated load, applied to act over a small portion on the top boundary is the prescribed traction. Material properties namely, Young's modulus (E) and Poisson's ratio (ν) are provided as inputs so that the Lamé parameters are expressed as,

$$\lambda = \frac{E\nu}{(1-2\nu)(1+\nu)} \; ; \qquad \mu = \frac{E}{2(1+\nu)}. \tag{2.6}$$

The displacement component $v(x, y)$ represents the depth of indentation. In this case, $v(x, y)$ corresponding to the node at the midpoint of a constituent section is relevant. With this information, the following indentation curves are plotted for varying stiffness ratios of the constituents, as a part of the parametric study.

Table 2.1. Average values of E and ν for some FRP constituents[4].

Material	Constituent	Young's modulus E (GPa)	Poisson's ratio ν
Carbon (Graphite)	Fiber	230	0.30
Glass[5]	Fiber	85	0.20
Aramid (Kevlar)	Fiber	124	0.36
Epoxy	Matrix	3.4	0.30

In general, fiber materials exhibit greater stiffness when compared to the matrix. The choice of stiffness ratios considered in this study is based on Table 2.1. $E_f/E_m > 20$ correspond to carbon/epoxy, glass/epoxy, and kevlar/epoxy composites while, in the case of polypropylene/epoxy composite (not listed in the table), E_f is comparable to E_m. A constant Poisson's ratio is picked for all constituents, since the parametric study involving variation of Poisson's ratio is not considered. The value corresponds to the Poisson's ratio of a glass/epoxy system with 45% fiber volume fraction (≈ 0.2). In the following discussion, results are presented and interpreted.

[4]Adapted from p.208 of [31].

[5]$E_x = E_y;\ \nu_{xy} = \nu_{yx}$.

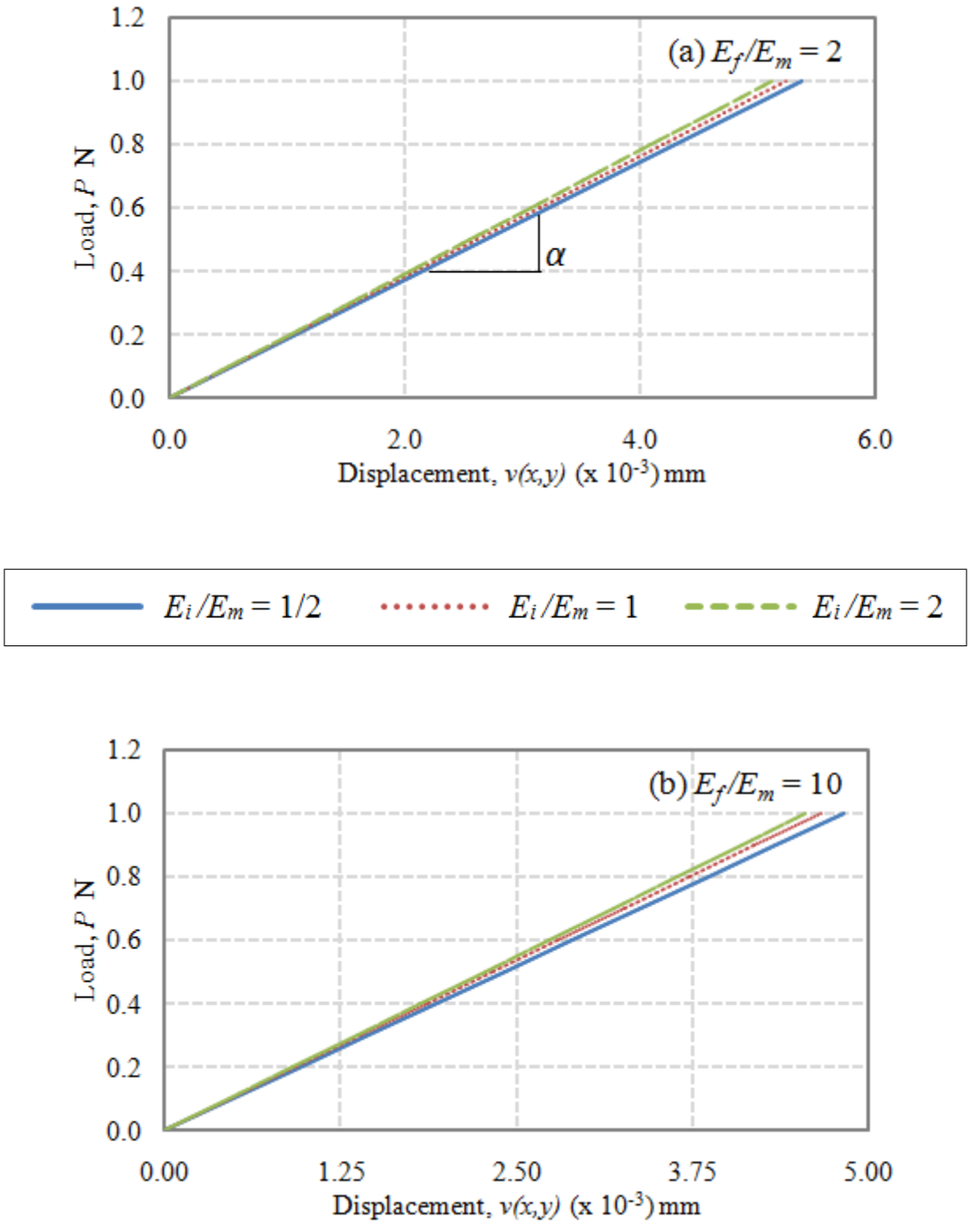

Figure 2.4. Indentation at the matrix for (a) $E_f/E_m = 2$ (b) $E_f/E_m = 10$ (c) $E_f/E_m = 50$ (d) $E_f/E_m = 100$.

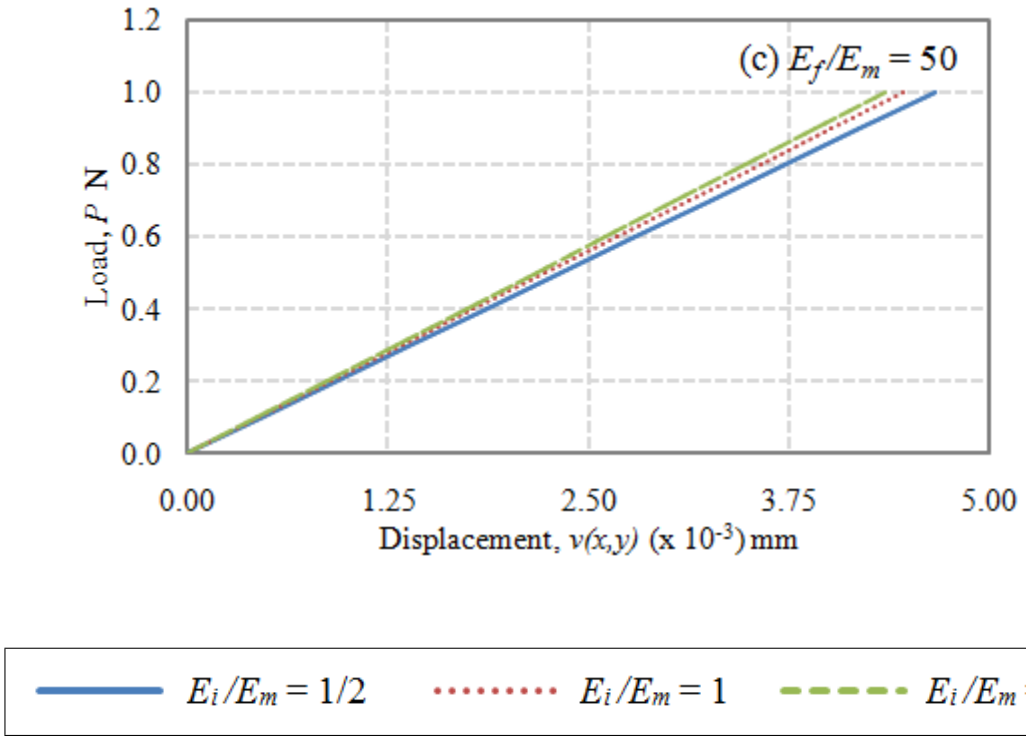

Figure 2.4. cont.

Figure 2.4 shows the load-displacement curves for indentation at the matrix for different stiffness ratios. The responses are a consequence of force ramps applied at a controlled rate of 1/10 on the matrix at its midsection, for fixed volume fractions of the constituents. Variation in the load-displacement responses are obtained for $E_f/E_m \leq 50$. This variation corresponds to increased slopes due to increased stiffness of the surrounding constituents. For $E_f/E_m > 50$, this variation is inconspicuous for a given E_i/E_m. The observed variations are likely to change with the loading location. This renders the mechanical characterization of matrix implausible. Though, an estimate of the average properties is possible for fixed volume fractions, a constant E_i/E_m and higher E_f/E_m (> 50), this approach is generally inapplicable. Because, in reality, the local volume fractions differ due to inhomogeneity in the material.

Table 2.2. Slope (α) under the load-displacement curves for indentation at the matrix.

E_f/E_m	E_i/E_m	$\alpha \times 10^3$
2	1/2	0.186
	1	0.191
	2	0.195
10	1/2	0.207
	1	0.215
	2	0.220
50	1/2	0.215
	1	0.224
	2	0.230
100	1/2	0.216
	1	0.225
	2	0.232

Table 2.2 presents a summary of the indentation response, defined by slope α. It is seen that, the overall matrix response is less senstitive to interphase properties. This is true when E_i/E_m is varied from 1/2 to 2 and is subjected to further verification for $E_i/E_m > 2$. When the fibers are much stiffer than the matrix, such as in carbon, glass, or kevlar fiber-reinforced polymer composites, the indentation response in polymers also insignificantly varies with the fiber stiffness. When the elastic stiffness of fiber is comparable to that of the matrix like in polypropylene fiber-reinforced polymer composites, mechanical response of matrix is quite sensitive to the fiber stiffness. Also, for all the cases tabulated above, α increases with E_i/E_m, which implies that a stiffer interphase contributes to an effective transfer of load from the matrix to the fiber. However, this contribution is barely noticeable in the presence of a very stiff fiber, like in a carbon/epoxy composite.

Magnitude of displacement, $|\mathbf{u}|$ and von Mises stress, T_v distribution at the peak load are extracted from ABAQUS as shown in Figure 2.5. The former is defined as:

$$|\mathbf{u}| = (\mathbf{u}.\mathbf{u})^{1/2}, \tag{2.7}$$

and the latter is calculated as mentioned in Appendix A.

As shown in Figure 2.5(a), $|\mathbf{u}| > 2.50\times10^{-3}\ mm$ in the immediate neighbourhood of the point of application of load and is confined to the matrix section. A small portion of the interphase is subjected to $|\mathbf{u}| = 1.25 \times 10^{-3}\ mm$, while fiber region experiences displacement magnitudes less than $1.25 \times 10^{-3}\ mm$. From Figure 2.5(b), a jump in the von Mises stress is observed. This is attributed to change of stiffness between the interphase and fiber sections.

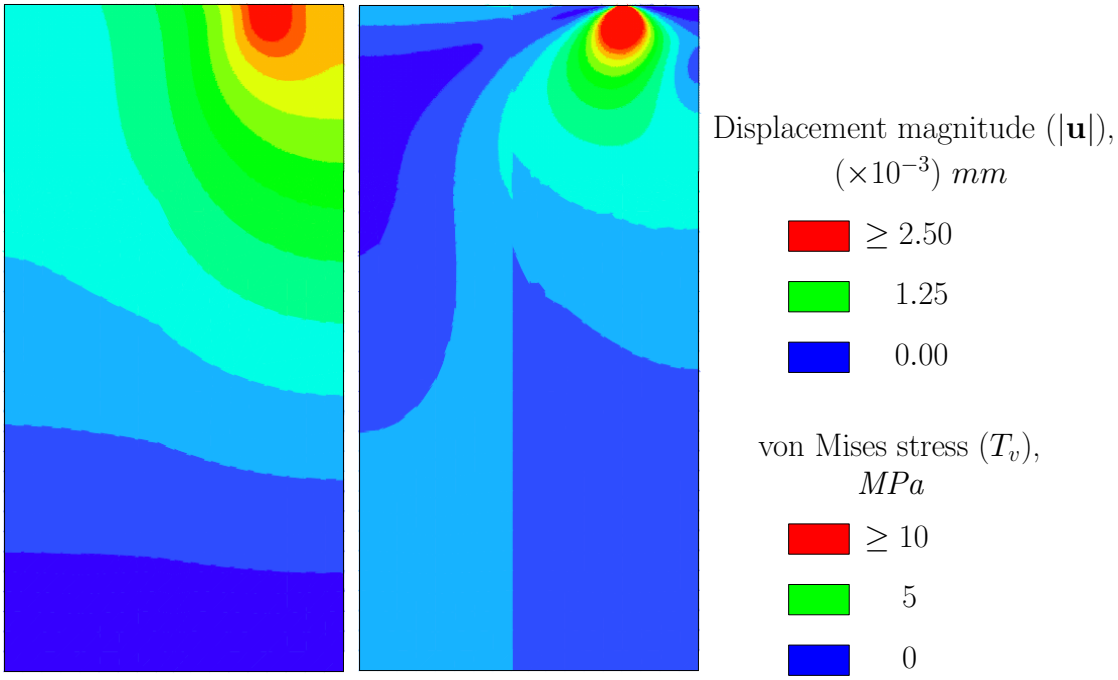

(a) Displacement plot, $|\mathbf{u}|_{max} = 5.24 \times 10^{-3}$ mm.

(b) Stress plot, $(T_v)_{max} = 505.45$ MPa.

Figure 2.5. Contour plots for indentation at the matrix ($E_f/E_m = 2$, $E_i/E_m = 1$) at maximum load, showing (a) displacement and (b) stress variations.

On the other hand, no such jump occurs at the interface between matrix and interphase regions because $E_i/E_m = 1$. $T_v \geq 5$ MPa in the upper one-fourth of the height of the matrix region, owing to a stiffer fiber together with $E_i/E_m = 1$.

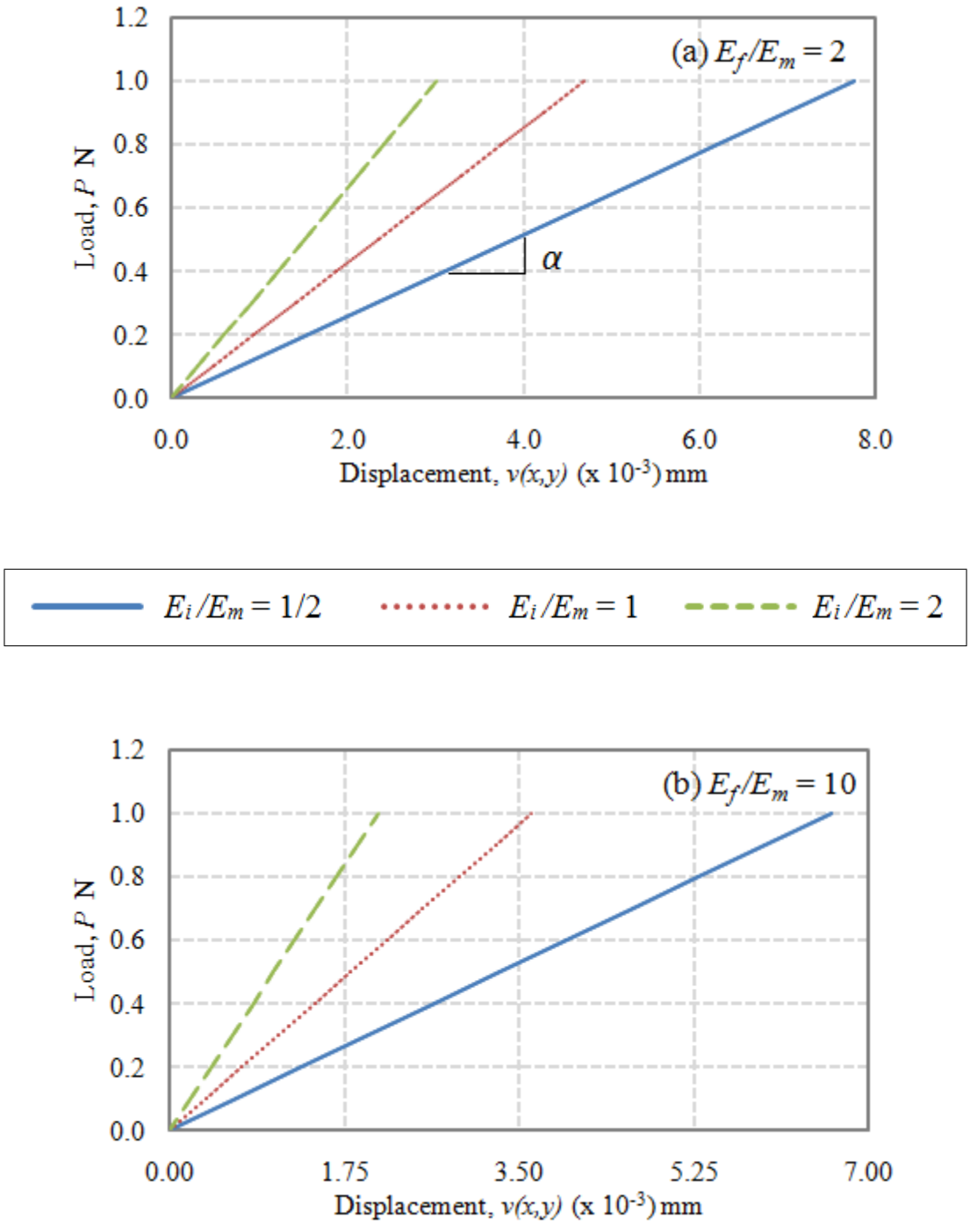

Figure 2.6. Indentation at the interphase for (a) $E_f/E_m = 2$ (b) $E_f/E_m = 10$ (c) $E_f/E_m = 50$ (d) $E_f/E_m = 100$.

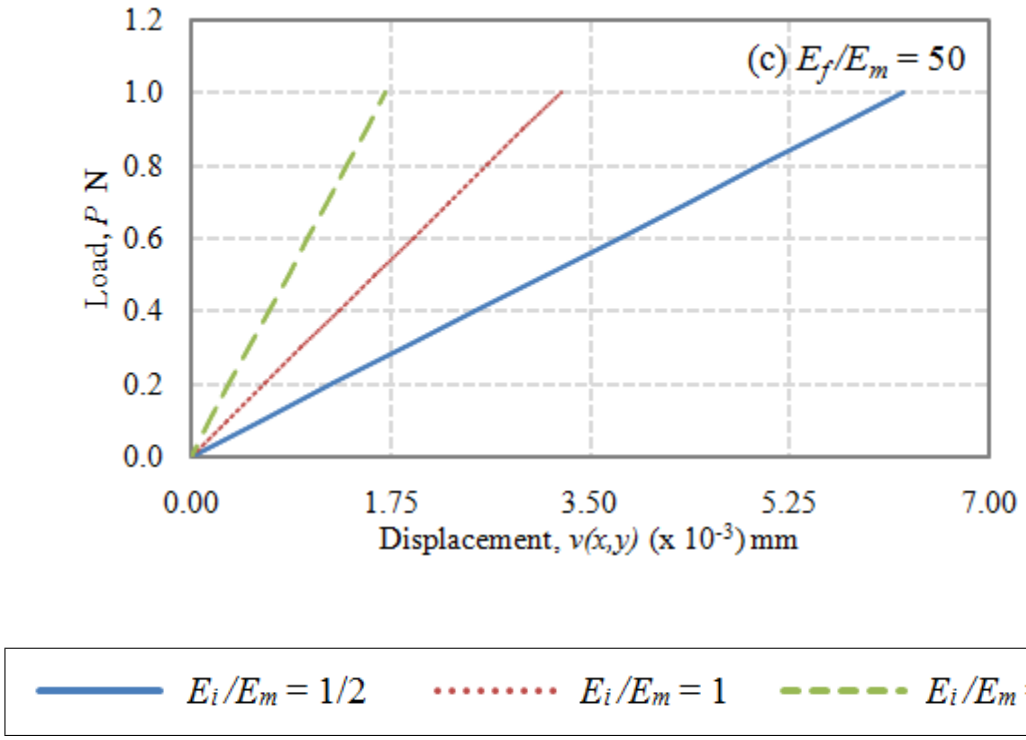

Figure 2.6. cont.

For indentation at the interphase (Figure 2.6), higher stiffnesses lead to greater slopes, based on a similar argument made for indentation at the matrix. Different responses are observed for varying E_f/E_m and E_i/E_m within the regimes simulated. It is seen that the localized response at the interphase varies significantly with properties of matrix and fiber. Characterization of interphase properties using indentation technique can therefore be challenging. Furthermore, interphase region is usually much smaller than the fiber and matrix regions. Since, indentation response is very sensitive to the loading location, extracting interphase properties from indentation is complicated. Thus, the use of indentation technique for an accurate characterization of real interphase properties in composites needs further investigation.

Table 2.3. Slope (α) under the load-displacement curves for indentation at the interphase.

E_f/E_m	E_i/E_m	$\alpha \times 10^3$
2	1/2	0.129
	1	0.214
	2	0.332
10	1/2	0.151
	1	0.276
	2	0.479
50	1/2	0.160
	1	0.308
	2	0.584
100	1/2	0.161
	1	0.314
	2	0.605

The responses are sensitive to variations in the constituent properties as seen from Table 2.3. Interphase response shows least variation for higher E_f/E_m (≥ 50) and lower E_i/E_m (< 1), although in reality, it is often not possible to know a priori, the stiffness of an interphase. It is interesting to note that, for known values of E_f and E_m, the increase in α is solely attributed to increasing stiffness of the interphase E_i. This enables characterization of the interphase if one succeeds in indenting the mid-section interphase despite their low volume fractions.

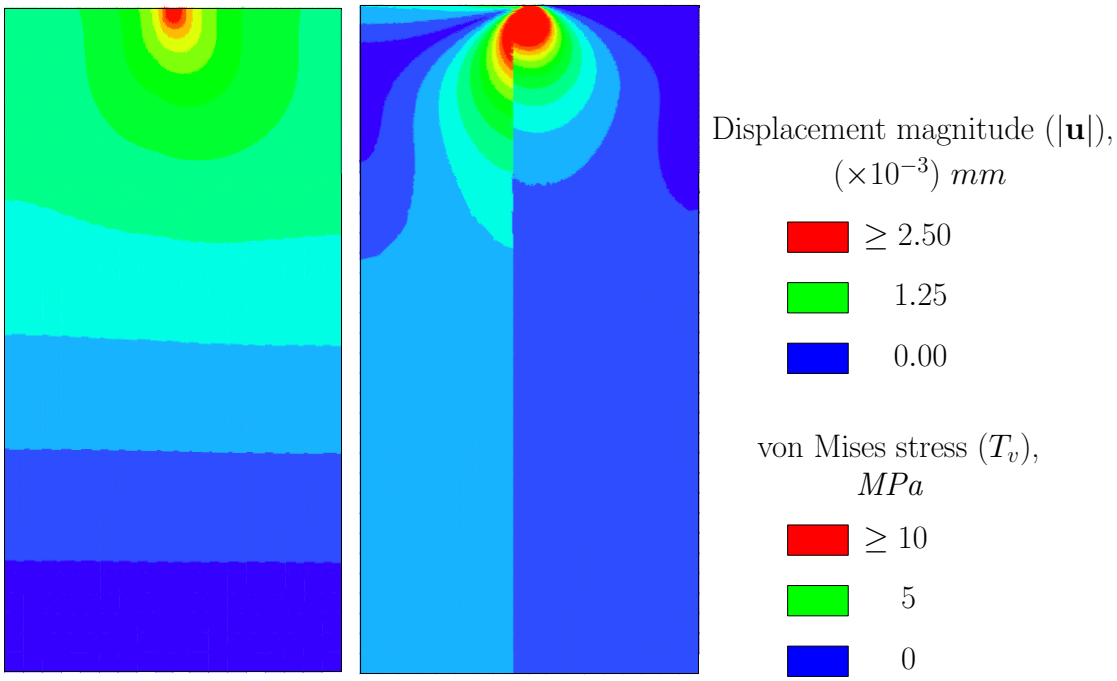

(a) Displacement plot, $|\mathbf{u}|_{max} = 4.69 \times 10^{-3}$ mm.

(b) Stress plot, $(T_v)_{max} = 505.65$ MPa.

Figure 2.7. Contour plots for indentation at the interphase ($E_f/E_m = 2$, $E_i/E_m = 1$) at maximum load, showing (a) displacement and (b) stress variations.

Displacement magnitudes greater than 1.25×10^{-3} mm are confined to the upper one-thirds of the geometry (Figure 2.7(a)) with the interphase taking up

$|\mathbf{u}| \geq 2.50 \times 10^{-3}\ mm$. Since $E_i/E_m = 1$ and perfect bonding exists between matrix-interphase sections, indentation at the interphase may be regarded as indentation at a different matrix location. The effect of loading location on the response is then clear from Figure 2.7. The variation in stiffness between adjacent constituents produces a prominent jump in the stresses at the interface between fiber and interphase regions (Figure 2.7(b)).

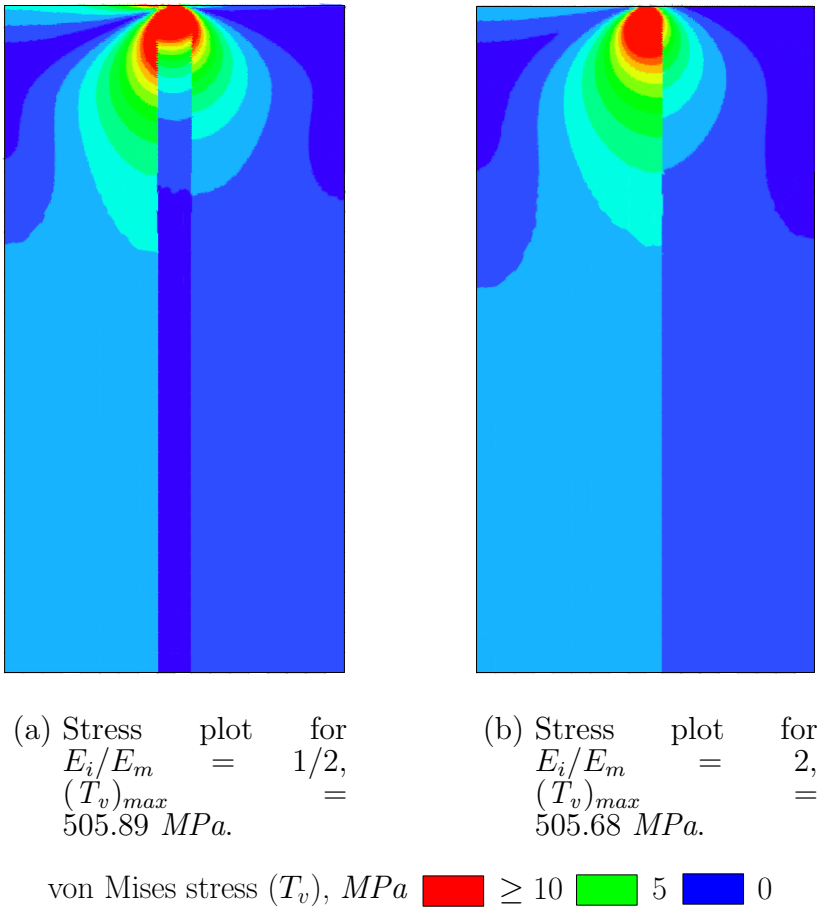

(a) Stress plot for $E_i/E_m = 1/2$, $(T_v)_{max} = 505.89\ MPa$.

(b) Stress plot for $E_i/E_m = 2$, $(T_v)_{max} = 505.68\ MPa$.

Figure 2.8. Contour plots for indentation at the interphase for $E_f/E_m = 2$ and maximum load, showing stress variations for (a) $E_i/E_m = 0.5$ and (b) $E_i/E_m = 2$.

Figure 2.8(a) shows that maximum stresses are witnessed in all the three constituents in the close vicinity of loading location. Stresses fade away gradually in the matrix and fiber regions for distances away from the interphase. Interphase is nearly stress-free in its lower regions due to the stiffer surrounding constituents. Fiber, possessing a higher stiffness, takes up more stresses than the matrix. Figure 2.8(b) is analogous to fiber indentation, but at a location other than the midsection. This is because $E_f/E_m = E_i/E_m = 2$. Stress jump is seen only at the interface between matrix and the interphase regions. Streses are of high magnitudes at regions of discontinuities which could result in debonding between the fiber and matrix. Debonding can occur either due to shear failure at the interface between fiber-interphase/matrix-interphase or due to shearing of the interphase itself. However, for a smaller interphase, this difference is barely noticeable. Hence, it might be possible to characterize the bonding strength of the fiber-matrix interphase.

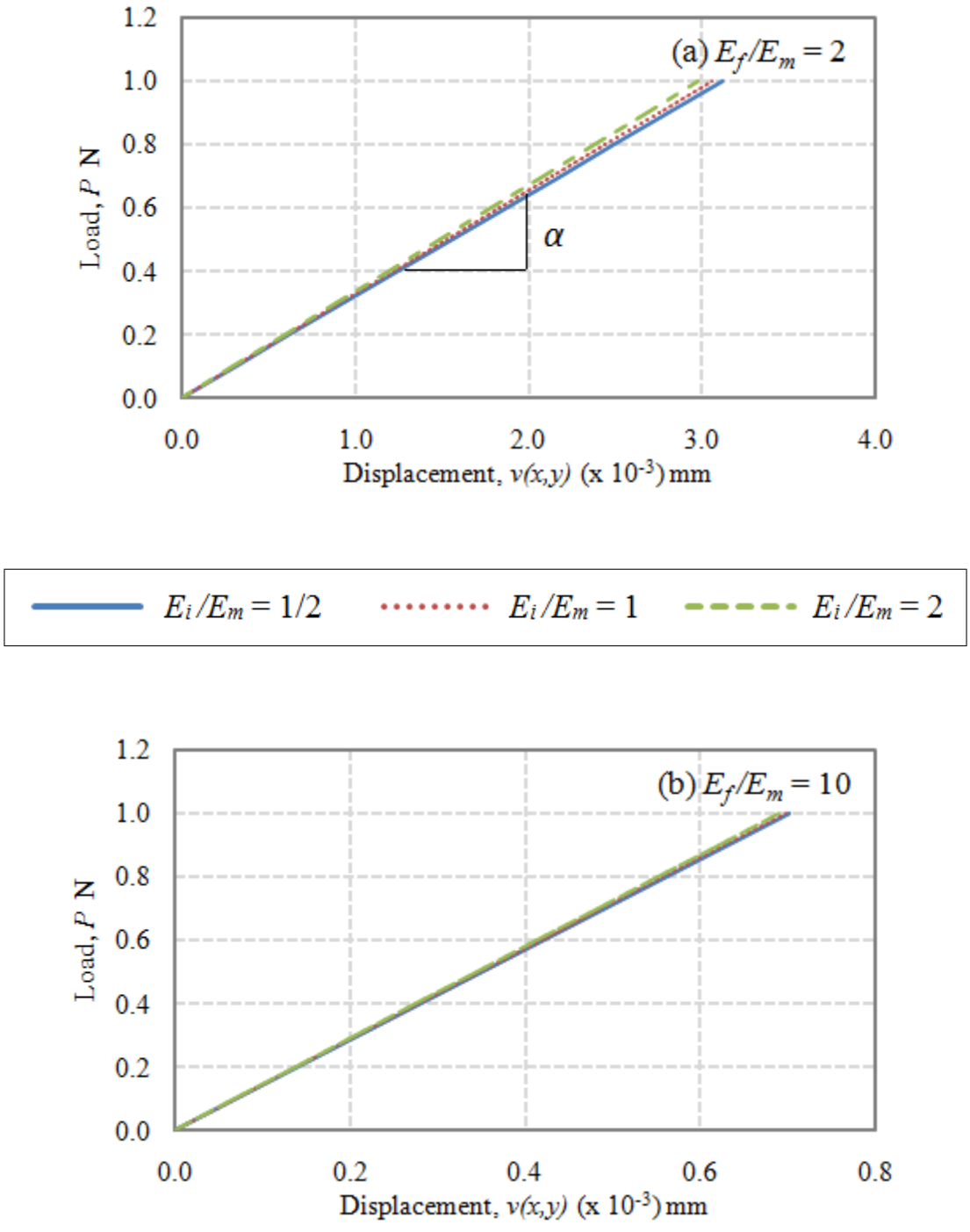

Figure 2.9. Indentation at the fiber for (a) $E_f/E_m = 2$ (b) $E_f/E_m = 10$ (c) $E_f/E_m = 50$ (d) $E_f/E_m = 100$.

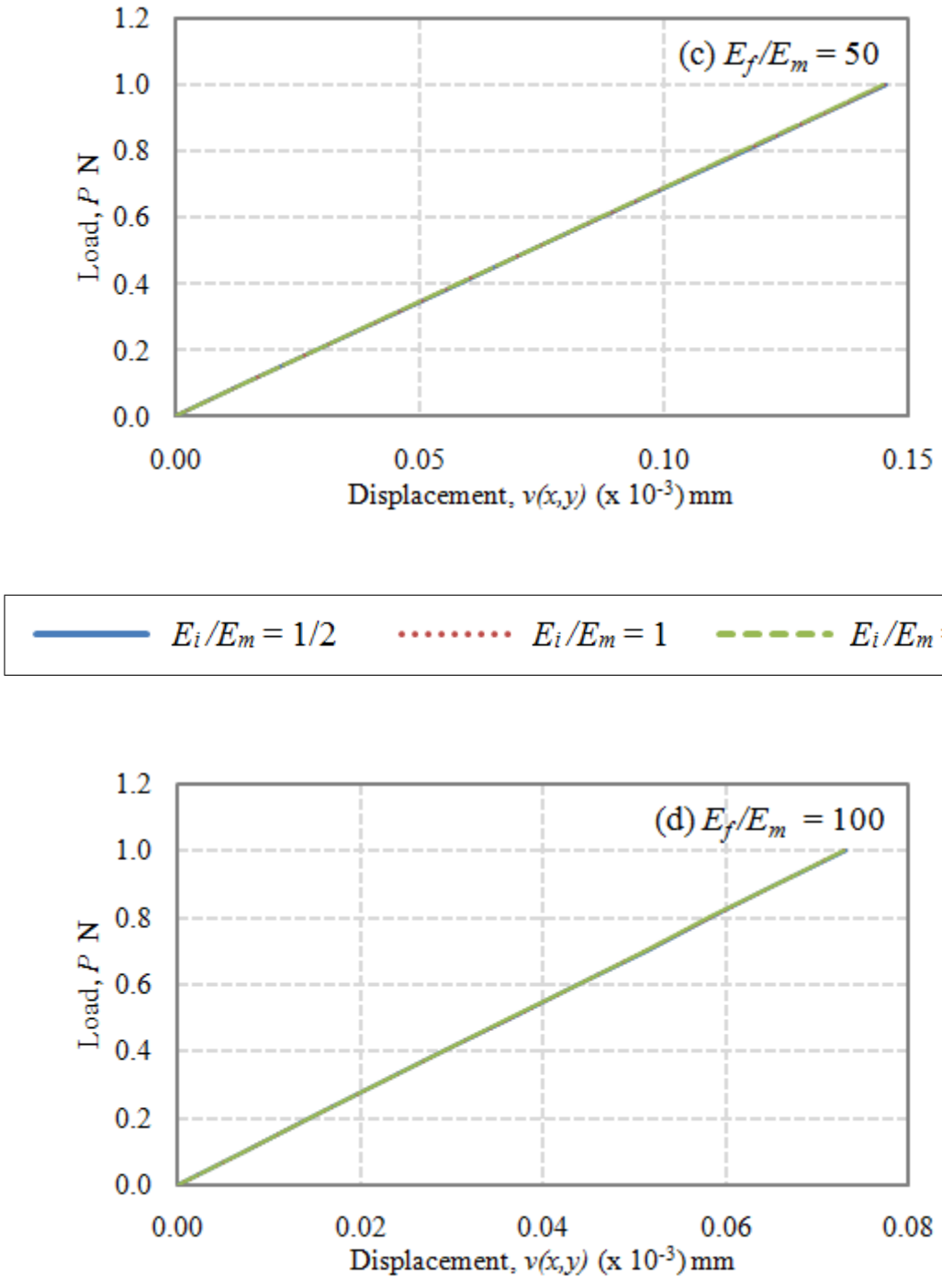

Figure 2.9. cont.

When the fiber is indented, variation in the load-displacement response with varying intephase stiffness are observed for $E_f/E_m \leq 10$, as illustrated in Figure 2.9. For $E_f/E_m > 10$, indentation response shows an unchanging trend for different E_i/E_m. If the loading location is moved closer to the interphase, changes in indentation response are expected. It seems feasible to characterize the modulus of fiber, provided the assumptions of linearized elasticity holds for all the constituents. With this rationale and the advantage of known fiber stiffness, back calculation of fiber modulus is attempted. Hence, *Flamant* solution for point load at the fiber is employed for $E_i/E_m = 1/2$, since the fiber response is seen to be insensitive to the surrounding constituents.

Table 2.4. Fiber stiffness for varying E_f/E_m.

E_f/E_m	$(E_f)_{Actual}$ MPa	$(E_f)_{Calculated}$ MPa
2	2000	≈ 1600
50	50000	≈ 33000
100	100000	≈ 65000

Table 2.4 gives a comparison between the actual fiber stiffness and that back calculated using the elasticity solution. Despite the insignificant effects of surrounding constituents on the fiber response, *Flamant* solution provides an ineffective means of back calculating fiber properties. The fact that *Flamant* solution is derived for a concentrated normal force on a homogeneous, elastic, infinite half-plane, explains its inapplicability to a finite domain problem with boundary conditions, which are

different from those associated with the *Flamant*'s problem.

Table 2.5. Slope (α) under the load-displacement curves for indentation at the fiber.

E_f/E_m	E_i/E_m	$\alpha \times 10^3$
2	1/2	0.320
	1	0.327
	2	0.336
10	1/2	1.423
	1	1.434
	2	1.449
50	1/2	6.873
	1	6.885
	2	6.903
100	1/2	13.681
	1	13.693
	2	13.711

Based on the slopes given by Table 2.5, the fiber response is insensitive to the properties of the surrounding constituents. Even for stiffness ratios as low as $E_f/E_m = 2$, changes in response at the fiber with varying interphase properties are not apparent. This kind of a response is verified only for E_i/E_m in the range 1/2 - 2. Variation of α with E_i/E_m for a given E_f/E_m is infinitesimal. This renders characterization of the fiber plausible when its response is assumed isotropic (generally not true). It is observed that α is directly proportional to E_f.

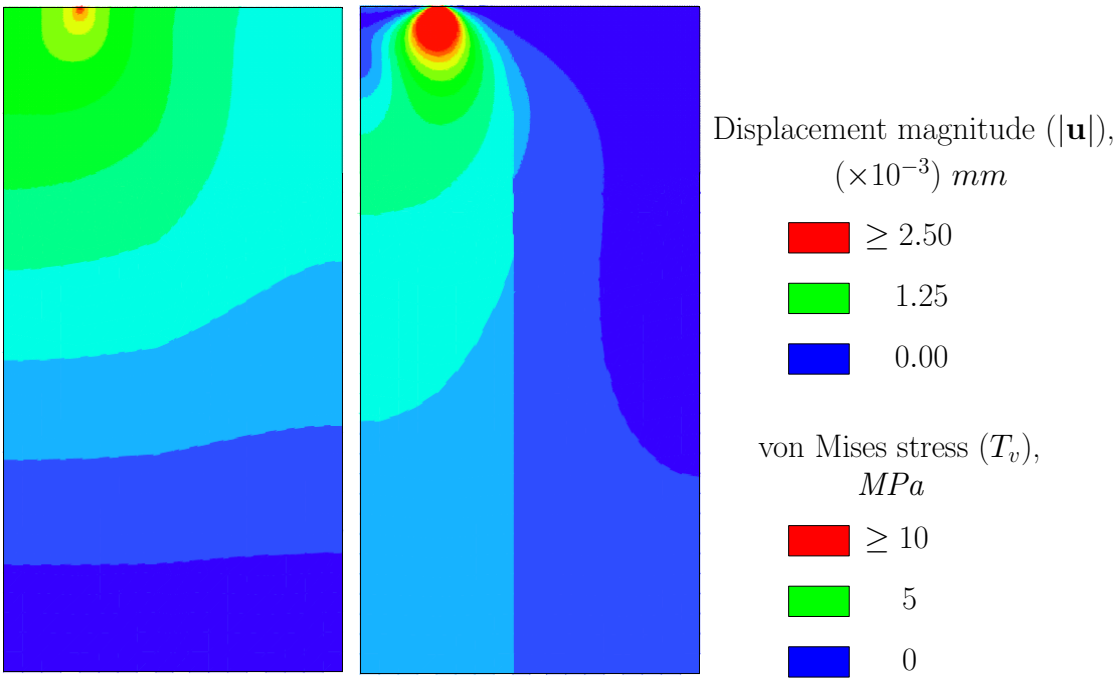

(a) Displacement plot, $|\mathbf{u}|_{max} = 3.06 \times 10^{-3}$ mm.

(b) Stress plot, $(T_v)_{max} = 505.54$ MPa.

Figure 2.10. Contour plots for indentation at the fiber ($E_f/E_m = 2$, $E_i/E_m = 1$) at maximum load, showing (a) displacement and (b) stress variations.

In Figure 2.10(a), $|\mathbf{u}| \geq 2.50 \times 10^{-3}$ mm corresponds to a very small region surrounding the loading location, while $|\mathbf{u}| \geq 1.25 \times 10^{-3}$ mm is limited to top one-thirds of the fiber region including a very small portion of the interphase. Stresses are mostly confined to the fiber region due to increased stiffness and they decrease gradually with distances away from the the indentation location (Figure 2.10(b)).

Thus, it can be seen that when the fiber is indented, field variables are faded away from point load, implying insignificant effect of the surrounding constituents on the local response. It is possible to calculate the slope $\alpha_{Exp.}$ using the experimental load-displacement data for indentation at the fiber. Then, one can extract FE load-displacement data by varying E_f until α_{FE} matches with $\alpha_{Exp.}$. E_f for a fiber stiffer than the matrix can be determined in this manner.

C. Coupled diffusion-deformation problem

An investigation on the effect of moisture concentration on indentation response is performed. It is assumed that the diffusion process follows Fick's laws. Both diffusion and deformation analyses make use of the same FE mesh (Figure 2.3). Displacement field due to indentation in the presence of moisture diffusing through the composite, from its top surface, (Figure 2.1) is determined by performing a sequentially coupled diffusion-deformation analysis. Unlike in a fully coupled analysis, the concentration field is not influenced by the deformation field.

Numerical solution to the following initial boundary value problem gives the moisture concentration $C(\mathbf{x}, t) = C(x, y, t)$ for all the nodes at all times until steady state is attained:

$$\frac{\partial C}{\partial t} = D \; div(\nabla C). \tag{2.8}$$

Equation (2.8) represents Fick's second law where, D is the diffusivity, which is assumed to be a constant in this study. It is necessary to mention that, in general, the diffusion process through polymers is non-Fickian [32].

$C(x, 1, t) = 1, \; \forall \; t > 0$ is the prescribed concentration at the top surface while the remaining segments are assigned zero flux boundary conditions i.e., $\frac{\partial C}{\partial x}(0, y, t) = \frac{\partial C}{\partial x}(0.5, y, t) = 0$ indicating that no moisture diffusion takes place normal to these edges and $\frac{\partial C}{\partial y}(x, 0, t) = 0$ representing that there is no moisture diffusion into or out of the bottom surface. Together, the flux boundary conditions enforce that the moisture diffusion takes place vertically from the top boundary to the bottom and confines moisture retention to the rectangular domain $\Omega : [0, 1/2] \times [0, 1]$. Initial condition for the concentration is given by $C(x, y, 0) = 0$.

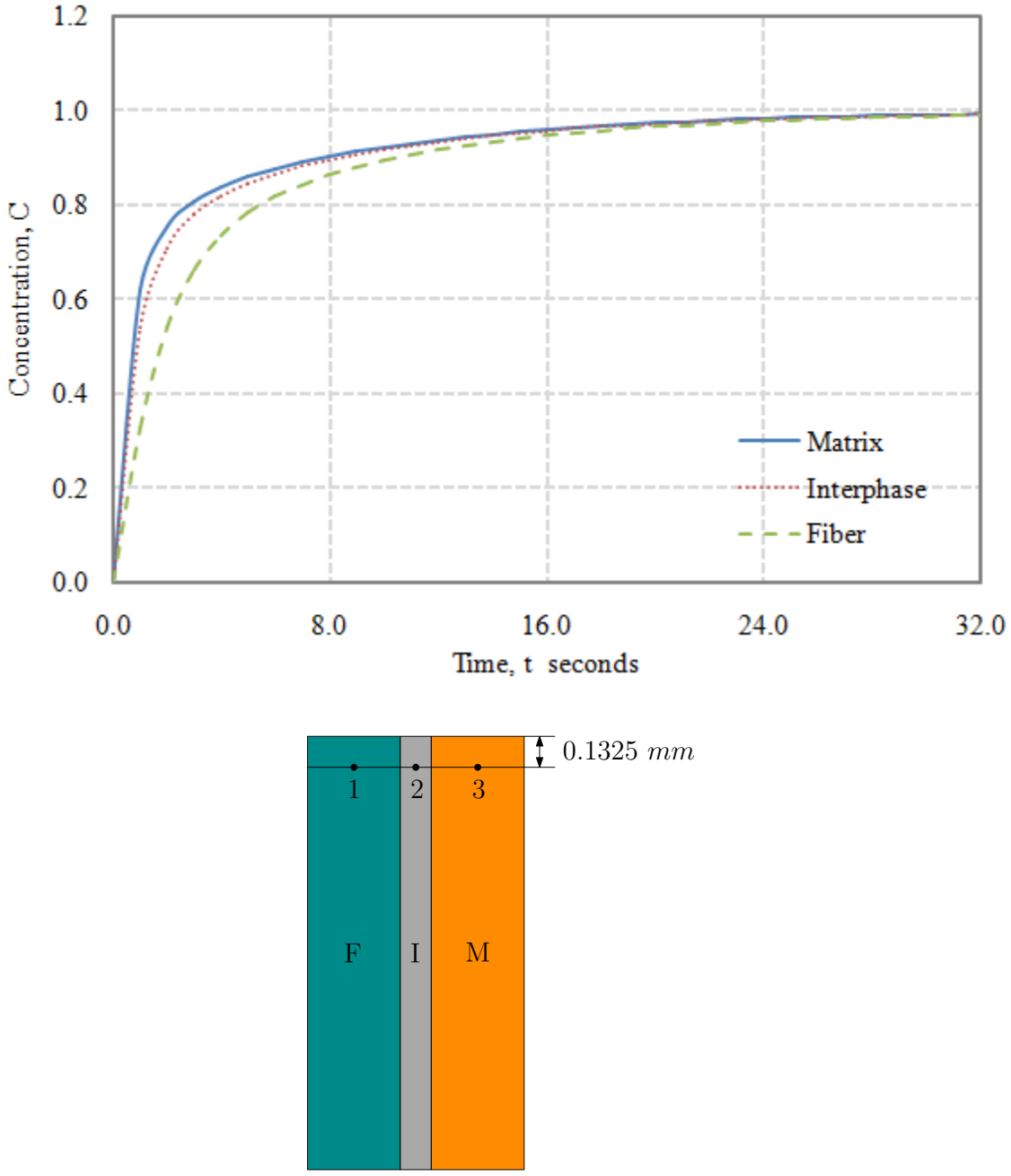

Figure 2.11. Variation of concentration at locations 1, 2 and 3 corresponding to matrix, interphase and fiber regions.

Figure 2.11 shows the concentration profiles for nodal locations 1, 2 and 3 in the fiber, interphase and matrix regions respectively, located at a distance of 0.1325 *mm* from the top surface. Discernible changes in concentration (upto 10^{-3}) occur until $t = 40$ *seconds*. Concentration changes are not very significant for $t > 40$ *seconds* before steady state is reached at around 112 *seconds*. In our case, steady state refers to the time before which the nodal concentrations are changing at a rate greater than 10^{-6}. Concentration profiles can be similarly plotted by picking different locations to demonstrate the significant concentration gradients at early times.

Subsequently, the deformation problem is solved as discussed in the previous section by introducing a concentration dependent elastic modulus,

$$E(C) = E(1 - 0.5C) \tag{2.9}$$

for each of the constituents such that the material degrades with increasing moisture content. It is possible to pick different forms for $E(C)$, as long as $E(C) > 0$. Poisson's ratio is assumed to remain a constant and effects of polymer swelling are ignored. Results are discussed in the following section.

A case of $E_f/E_m = 2; E_i/E_m = 1$ is picked for studying the effect of concentration on the load-displacement curves (Figure 2.12). Loading and unloading curves do not coincide with slower deformations leading to lower slopes. Continuously changing material moduli due to moisture diffusion gives different loading and unloading paths.

Even with the onset of material degradation, the constituents are stiffer at early times than at times approaching steady state. Thus, the load-displacement curves exhibit higher slopes for faster loading rates. The distinction between loading and unloading curves is prominent at loading rates of 1/10 and 1/20. The concentration changes being significant at early times (Figure 2.11), bring about greater variations in the material moduli until $t = 40$ *seconds*.

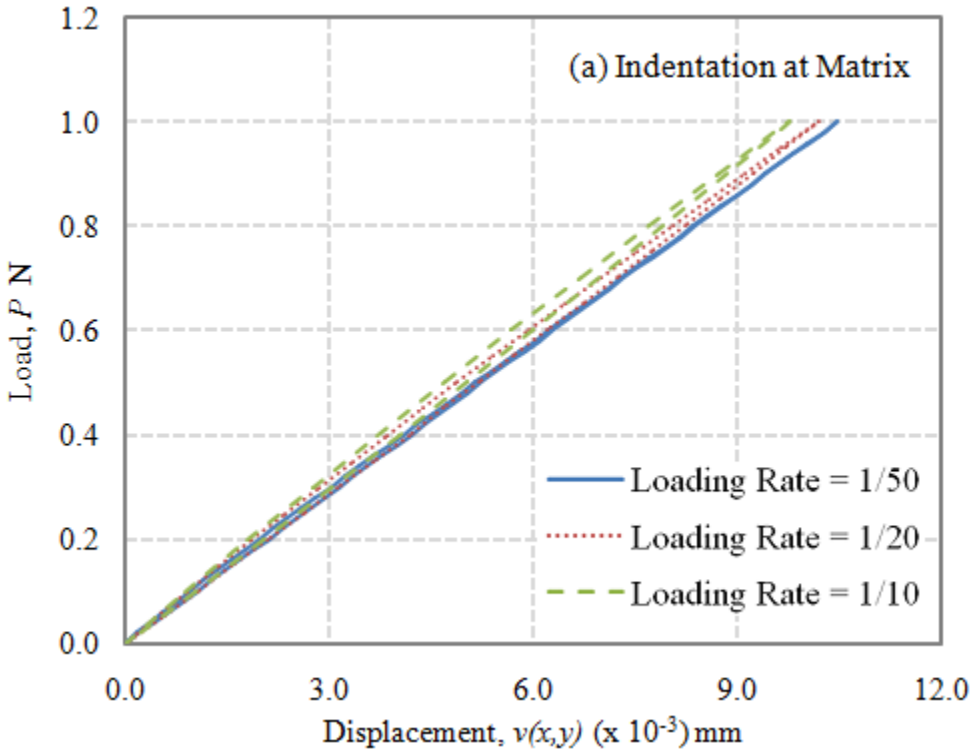

Figure 2.12. Effect of loading rates with $E_f/E_m = 2$ and $E_i/E_m = 1$ for indentation at (a) matrix (b) interphase (c) fiber.

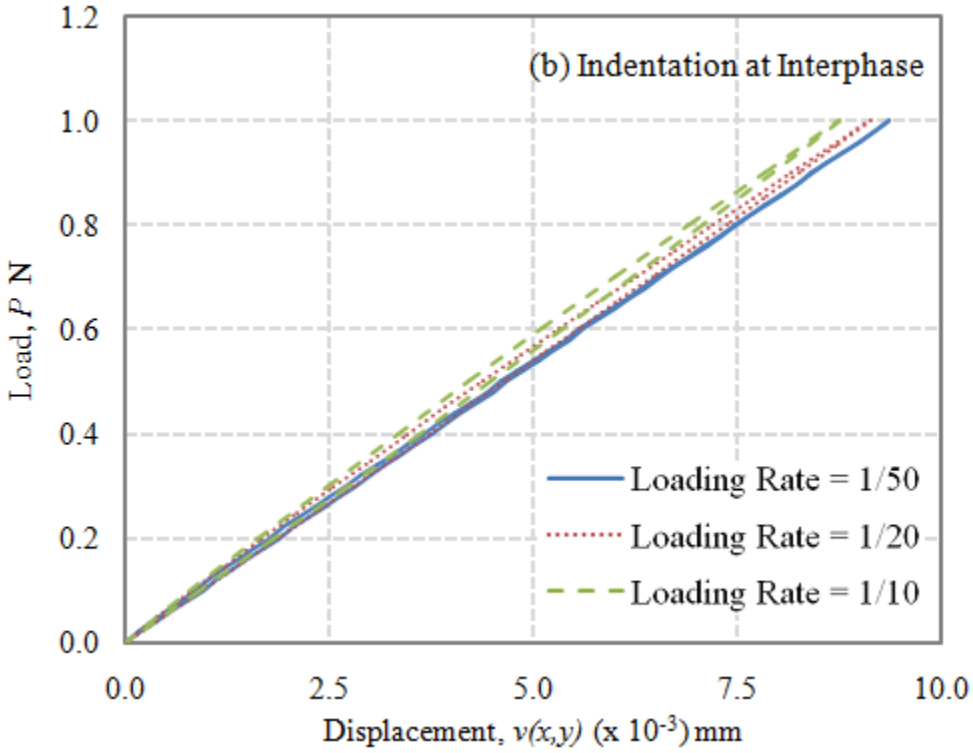

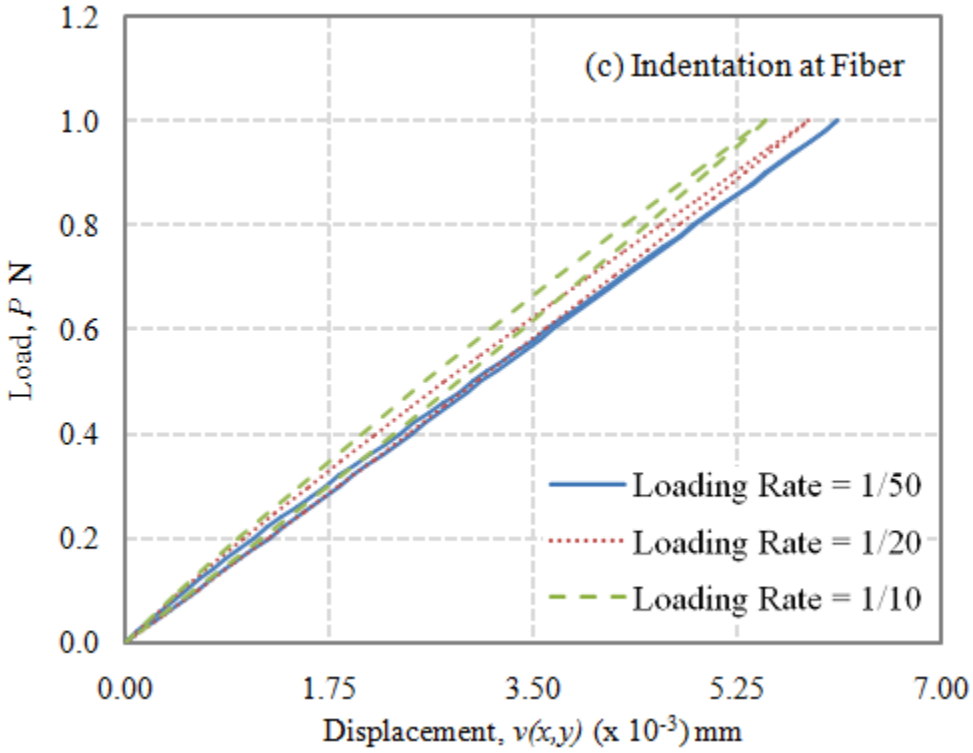

Figure 2.12. cont.

Though the elastic moduli for all the constituents are reduced to half their original value while they are degraded, variations are pronounced for indentation at the fiber. This is attributed to a greater change in the modulus of fiber when compared to that of matrix or interphase. However, these responses are with respect to the elastic properties of the constituents degrading with concentration. Since, the concentration gradients are smaller for $t > 40$ *seconds*, the corresponding changes in the material moduli is inconspicious. This renders the distinction between loading and unloading curves unclear for loading rate greater than 1/20.

Table 2.6. Average slope (α_{avg}) under the load-displacement curves for indentation at the interphase ($E_f/E_m = 2$, $E_i/E_m = 1$) with an elastic matrix and moisture diffusion.

Loading Rate	$\alpha_{avg} \times 10^3$
1/50	0.107
1/20	0.110
1/10	0.114

Table 2.7. Average slope (α_{avg}) under the load-displacement curves for indentation at the fiber ($E_f/E_m = 2$, $E_i/E_m = 1$) with an elastic matrix and moisture diffusion.

Loading Rate	$\alpha_{avg} \times 10^3$
1/50	0.164
1/20	0.171
1/10	0.182

Though the loading and unloading curves are different, this difference is not significant. This permits calculation of an average slope (α_{avg}) of these curves, as if they were straight lines. The average slopes so determined, are tabulated in (Table 2.6 and Table 2.7) shown above. Faster loading would mean steeper slopes, since the constituents are more stiffer at early times. Comparing α_{avg} for the case of moisture diffusion with α from Table 2.3 and Table 2.5 (without moisture diffusion), $\alpha/\alpha_{avg} \approx 2$ for the loading rates simulated. This implies that the diplacements in the saturated condition are twice the displacements in dry condition.

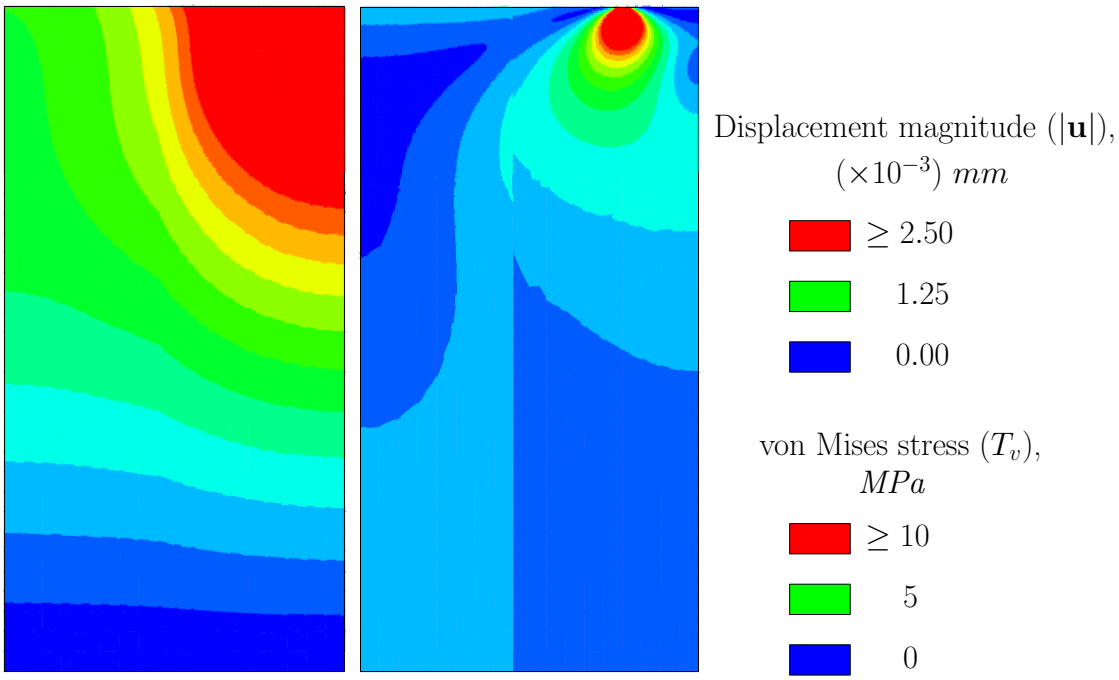

(a) Displacement plot, $|\mathbf{u}|_{max} = 10.205 \times 10^{-3}$ mm.

(b) Stress plot, $(T_v)_{max} = 505.478$ MPa.

Figure 2.13. Contour plots for indentation at the matrix ($E_f/E_m = 2$, $E_i/E_m = 1$) with moisture diffusion at maximum load (Loading Rate=1/20), showing (a) displacement and (b) stress variations.

Figure 2.13(a) depicts observable changes in displacement field in the presence of moisture diffusion, as opposed to Figure 2.5(a) of section B, for indentation at the matrix.

Higher diffusivity of the matrix material when compared to the interphase and fiber, causes faster degradation of the modulus due to increased moisture concentrations at early times. Lower modulus results in a more complaint matrix due to the presence of moisture when compared to the dry condition. This explains the large displacement magnitudes near the top surface of matrix region, when the matrix material is pushed by a point load. It is noted that the maximum displacement in the matrix region due to concentration of fluid is twice as large as that in the dry condition, since the modulus decreases by half at the saturated condition, which is expected. Stress variation on the other hand (Figure 2.13(b)) looks more or less the same as in Figure 2.5(b). Owing to loss of stiffness in saturated condition, the material actually requires a smaller stress to experience the displacement magnitude shown in Figure 2.5. Since the admissible displacements due to a softer material increase twofold, a nearly constant stress level ($\approx 505.45\ MPa$) is maintained.

CHAPTER III

INDENTATION RESPONSE WITH A LINEAR VISCOELASTIC MATRIX

Practicality dictates that the mechanical response of polymeric matrix in a FRP composite is not that of a linearized elastic solid. Creep and stress relaxation phenomena in polymers, linear or non-linear, can be pronounced, affecting overall response of the composite. Consequently, indentation response of the FRP constituents is examined when the polymer matrix is modeled as a linear isotropic viscoelastic solid-like material. The effect of aging on the constituents are not considered. The other two constituents are assumed isotropic, linear elastic with respect to their mechanical response. Despite the preceding assumption, viscoelastic behaviour of the surrounding polymer matrix might affect the localized response during indentation.

In this chapter, the purpose is to examine the effects of a linear viscoelastic matrix on the localized response during indentation in fiber, matrix and interphase regions for different loading rates. The same two-dimensional model of the FRP composite with 45% fiber volume content is considered (Figure 2.1). Indentation is performed on the center of each constituent separately in the micro-section of the composite, by application of a unit magnitude point load.

First part of this chapter deals with the effect of loading rates for the deformation problem. The second part focuses on the effect of moisture concentration and indenter tips on the indentation response.

A. Deformation problem

Indentation at the matrix, interphase and fiber sections are analyzed, one at a time for different loading rates. Problem description and modeling of Chapter II A holds and the procedure listed in Chapter II B is adopted as far as loading is concerned.

The elastic moduli for fiber (E_f) and interphase (E_i) are expressed in terms of the instantaneous elastic modulus for the polymer matrix (E_0), chosen to be 1000 MPa. Poisson's ratio (ν) is held constant ($= 0.2$) for all constituents including the polymer (viscoelastic) matrix.

The polymer matrix is modeled as a linear isotropic viscoelastic solid-like material. Mechanical analog for the desired response in one-dimension is constructed using N Kelvin-Voigt (a spring and a viscous damper in parallel: mechanical analog for viscoelastic solid-like response) elements with a spring (mechanical analog for linear elastic solid) in series (Figure 3.1).

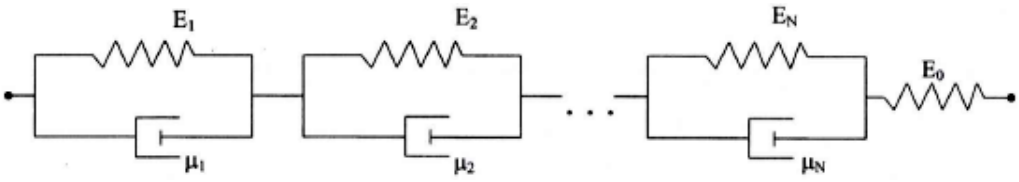

Figure 3.1. Mechanical analog for one-dimensional viscoelastic response of the polymer matrix[6].

Creep compliance for this model takes the form of a Prony series:

$$D(t) = \frac{1}{E_0} + \sum_{i=1}^{n} \frac{1}{E_i}(1 - e^{-t/\tau_i}) \ , \tag{3.1}$$

where $\tau_i = \mu_i/E_i$, called the retardation time. If $T(t)$ and $\varepsilon(t)$ denote the stress (normal or shear) and strain (normal or shear) respectively at time t, the creep form of the constitutive equation for one-dimensional response of linear isotropic viscoelastic

[6]Adapted from p.53 of [33].

material reads:

$$\varepsilon(t) = T(0)D(t) + \int_0^t D(t-s)\dot{T}(s)\, ds = T * dD \ , \tag{3.2}$$

$(*)$ representing the convolution of $T(t)$ and $D(t)$.

Based on Equation (3.2), the constitutive relations for two-dimensional response of an isotropic linear viscoelastic material with constant Poisson's ratio is written as

$$\varepsilon_{xx} = [T_{xx} - \nu T_{yy}] * dD; \quad \varepsilon_{yy} = [T_{yy} - \nu T_{xx}] * dD; \quad \varepsilon_{xy} = 2T_{xy} * dJ. \tag{3.3}$$

$J(t)$ is the creep compliance in shear and is given by $J(t) = 2(1+\nu)D(t)$, for a constant ν.

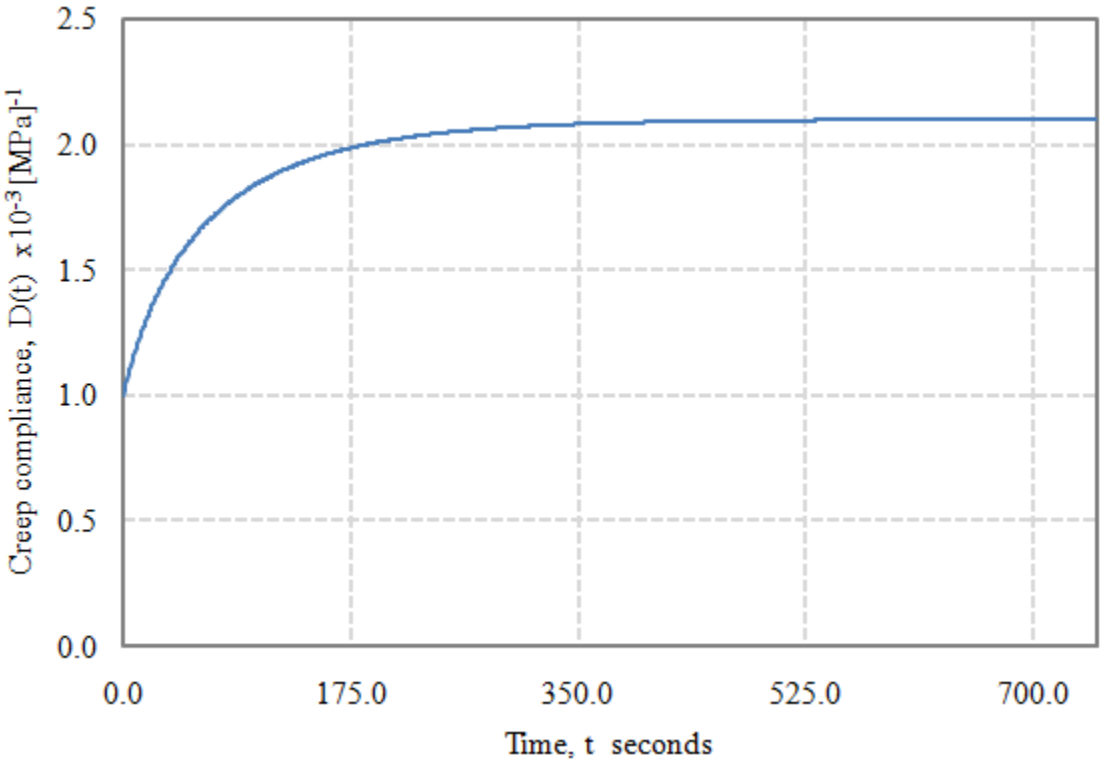

Figure 3.2. Creep compliance curve for N (=4) Kelvin-Voigt elements with a spring in series.

Equations (3.3) are implemented through a FORTRAN subroutine (UMAT) in ABAQUS, to obtain a numerical solution. This code defining the constitutive relations for time-dependent behaviour of the viscoelastic material was developed by Muliana et al. [34]. First five terms of the Prony series ($N = 4$) are considered in Equation 3.1 for the polymer matrix material property defintion. The constants are chosen to be $1/E_i = 5 \times 10^{-5}, 1.5 \times 10^{-5}, 3 \times 10^{-5}, 6 \times 10^{-5}$ and $\tau_i = 10, 25, 50, 100$ for $i = 1, 2, 3, 4$ respectively and the variation of $D(t)$ with time is as shown in Figure 3.2. Results for the deformation problem involving a viscoelastic matrix are now discussed.

Due to the influence of viscoelastic behaviour exhibited by the surrounding polymer matrix, loading and unloading paths do not coincide, even when the elastic constituents are indented. The difference is more prominent for a loading rate of 1/100 as seen in Figure 3.3, since the change in creep compliance for the polymer matrix (Figure 3.2) is more prominent until $t = 200$ *seconds*. A faster loading rate of 1/10 also shows an observable difference between loading-unloading curves with steeper slopes, because the time rate of change of creep compliance is higher at early times. For slow loading (1/1000), since the creep compliance curve becomes asymptotic for $t = 750$ *seconds*, a minimum difference between the loading and unloading paths is observed. When loading is very slow compared to the creep time, creep compliance reaches a constant value i.e., $D(t) \to D(\infty)$ as $t \to \infty$, resulting in a more compliant response of the polymer matrix. In addition, the displacement is nearly zero upon the removal of load. This is typical of a viscoelastic solid-like material which generally recovers all the strain over a sufficiently long time, once the stress is removed.

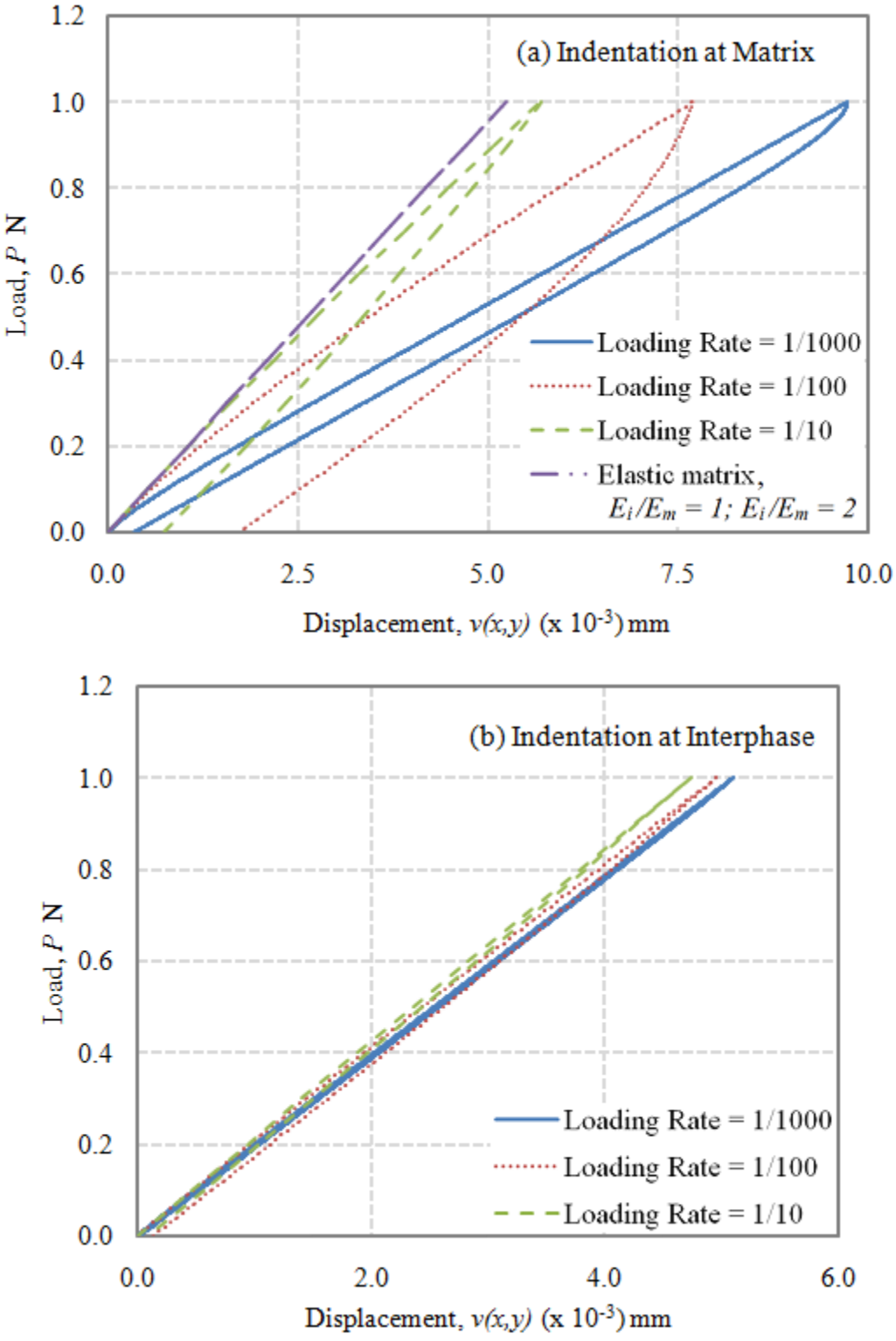

Figure 3.3. Effect of loading rates for indentation at (a) matrix (b) interphase, $E_i/E_0 = 1$ (c) fibre, $E_f/E_0 = 2$.

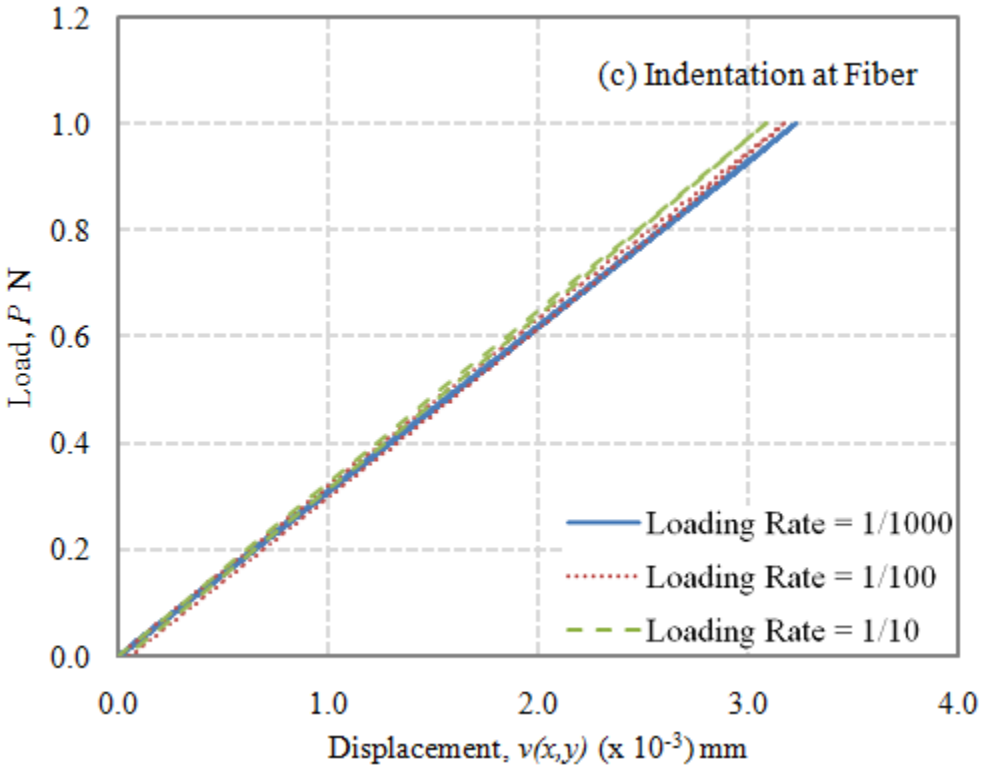

Figure 3.3. cont.

Table 3.1. Average slope (α_{avg}) under the load-displacement curves for indentation at the interphase ($E_f/E_0 = 2$, $E_i/E_0 = 1$) with a viscoelastic matrix.

Loading Rate	$\alpha_{avg} \times 10^3$
1/1000	0.196
1/100	0.202
1/10	0.211

Figure 3.3(a) also includes load-displacement curve for the elastic matrix for the purpose of comparison. It is to be recalled that matrix characterization was rendered implausible when its mechanical behaviour was assumed linear elastic. The

viscoelastic responses are prominent even for a very slow loading rate of 1/1000 with considerable differences in slopes. Viscoelastic repsonses for different loading rates show large deviations from the elastic response. Hence, it might not be feasible to characterize the polymer matrix by indentation though the surrounding constituents are elastic. Also, the fast loading rate of 1/10 better resembles the the elastic response.

Table 3.2. Average slope (α_{avg}) under the load-displacement curves for indentation at the fiber ($E_f/E_0 = 2$, $E_i/E_0 = 1$) with a viscoelastic matrix.

Loading Rate	$\alpha_{avg} \times 10^3$
1/1000	0.310
1/100	0.316
1/10	0.324

For indentation at interphase and fiber, the effect due to loading rates is insignificant. An average slope (α_{avg}) is calculated for a set of loading-unloading curves corresponding to each loading rate, as done in chapter II. This is given by Table 3.1 and Table 3.2 for indentation at interphase and fiber respectively. When compared with α for the case of elastic matrix ($E_f/E_m = 2$, $E_i/E_m = 1$) from Tables 2.3 and 2.5, $\alpha_{Em}/(\alpha_{avg})_{Vm} = 1.009$ when the loading is faster (1/10). For slower rates of loading, $\alpha_{Em}/(\alpha_{avg})_{Vm} = 1.09$ (Em: Elastic matrix; Vm: Viscoelastic matrix).

This indicates that, for fast loading, displacements at the interphase and fiber regions with a viscoelastic matrix are comparable to the corresponding displacements with an elastic matrix. Displacement increases by 10% as the loading rate is decreased to 1/1000. Hence, estimation of elastic properties of fiber and interphase through indentation is credible in the presence of a polymer matrix, provided the loading is faster i.e., the response of fiber and interphase can be approximated only in the presence of an elastic matrix. Once the viscoelastic effects become prominent, it is not feasible to extract the elastic properties of fiber and interphase.

When the polymer matrix is indented, displacement and stress distributions change as compared to the distributions obtained with indentation on a linearly elastic matrix (Figure 2.5). There is a marginal increase in $|\mathbf{u}|_{max}$, while the increase in $(T_v)_{max}$ is much higher. The viscoelastic matrix creeps faster at early times (Figure 3.2) resulting in higher deformations.

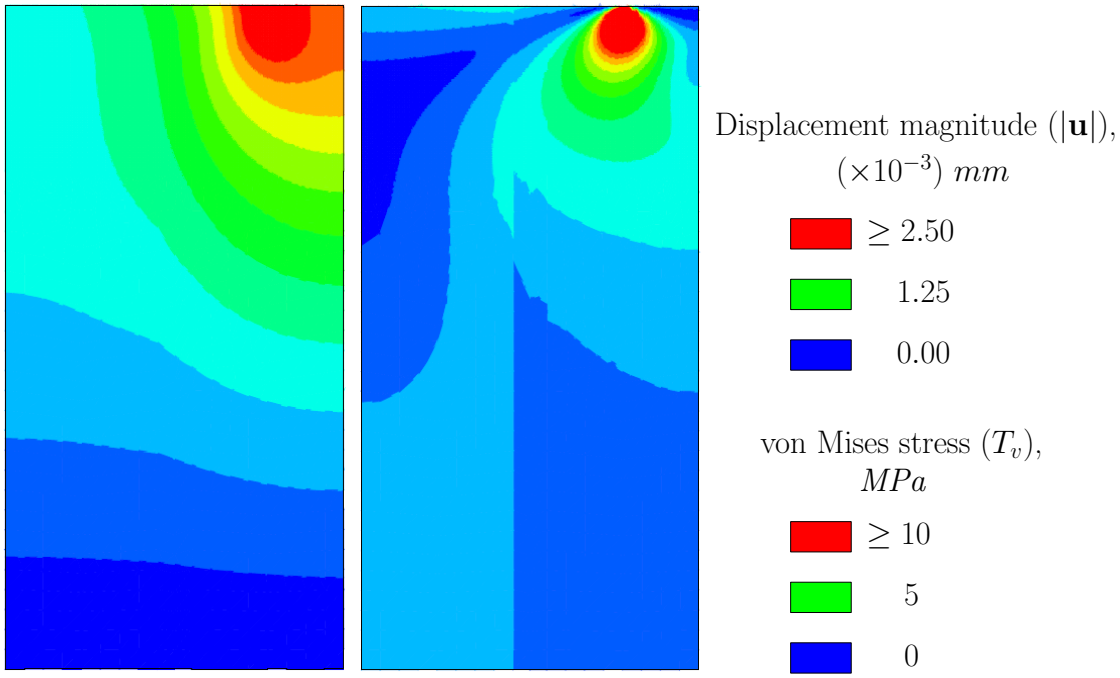

(a) Displacement plot, $|\mathbf{u}|_{max} = 6.077 \times 10^{-3}$ mm.

(b) Stress plot, $(T_v)_{max} = 522.076$ MPa.

Figure 3.4. Contour plots for indentation at the viscoelastic matrix ($E_f/E_0 = 2$, $E_i/E_0 = 1$) at maximum load (Loading Rate = 1/20), showing (a) displacement and (b) stress variations.

B. Coupled diffusion-deformation problem

Solution to the initial boundary value problem from Chapter II C is used in a sequentially coupled analysis. The dependence of material moduli on concentration is introduced by the same relation as used earlier with $\beta^m = 0.5$, corresponding to instantaneous elastic modulus for the polymer matrix i.e.,

$$E_0(C) = E_0(1 - 0.5C) \ . \tag{3.4}$$

Based on the time-temperature superpostion principle for a thermo-rheologically simple material, an expression for the creep response of a linear viscoelastic material, with respect to time t and moisture concentration C can be analogously written. This is because, the evolution of temperature or concentration with time, across a region, is described by the same governing equation. Let C_0 denote the reference concentration corresponding to the dry condition ($C = 0$) and C_1 be the steady state concentration corresponding to the saturated condition ($C = 1$). Also, let $D(t, C_0)$ and $D(t, C_1)$ be the creep compliances corresponding to uniform moisture conditions (similar to isothermal conditions for temperature) $C = 0$ and $C = 1$ respectively. For a known $D(t, C_0)$, $D(t, C_1)$ is obtained by invoking the aforesaid time-temperature superposition:

$$D(t, C_1) = D\left(\frac{t}{a(C_1, C_0)}, C_0\right). \tag{3.5}$$

$a(C_1, C_0)$ is called the shift function which is equal to unity for $C_1 = C_0$. It is assumed that the polymer matrix creeps faster at higher concentrations. Therefore, $a(C_1, C_0) < 1$ indicating shorter time for $D(t)$ to attain a particular value. Thus, Equation (3.5) enables to determine the response at $C = 1$ when the response at $C = 0$ is known or vice-versa.

For transient moisture diffusion with time-dependent concentration profiles, Equation (3.5) takes the form:

$$D[t, C(s)_{s=0}^{t}] = D\left[\int_0^t \frac{ds}{a(C(s), C_0)}, C_0\right]. \tag{3.6}$$

$\int_0^t \frac{ds}{a(C(s),C_0)} = \zeta(t)$ is referred to as the reduced time. This is valid for thermo-

rheologically simple materials.

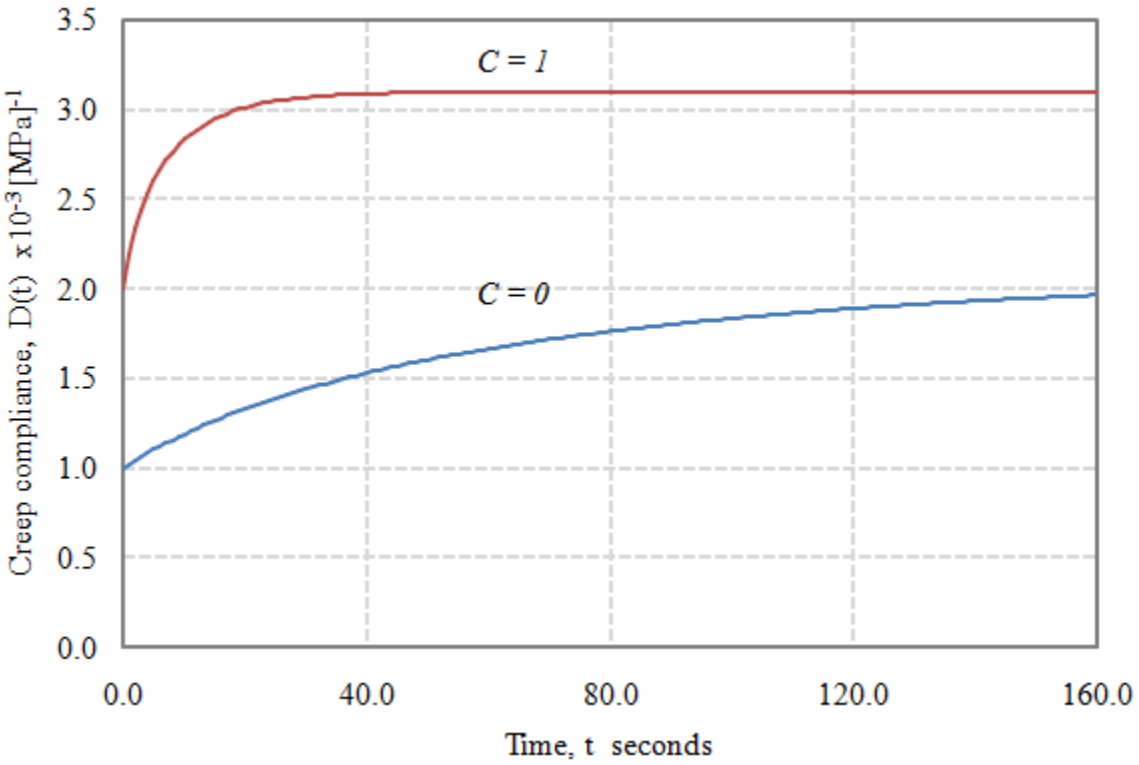

Figure 3.5. Creep compliance for different concentrations.

The concentration dependent creep compliance can therefore be written as:

$$D(t,C) = \frac{1}{E_0(C)} + \sum_{i=1}^{n} \frac{1}{E_i}(1 - e^{-\zeta(t)/\tau_i}) \ , \tag{3.7}$$

with the shift function, $a\big(C(s), C_0\big) = 1/\big(1{+}9C(s)\big)$. Different forms for shift function can be constructed. In this study, shift function is chosen such that $a(C_1, C_0) < 1$, since the polymer is assumed to creep faster for higher values of concentration. The FORTRAN subroutine is modified to handle Equations (3.4) and (3.7) for the coupled problem involving a polymer matrix. Figure 3.5 depicts the variation of $D(t)$ with time at fixed concentrations C_1 and C_0.

For indentation at the matrix, it is observed from Figure 3.6, that loading and unloading curves exhibit prominent differences for faster loading. This is expected, since the concentration changes as well as time rate of change of creep are significant at early times. For loading rate 1/50, the displacement is nearly zero, when matrix is unloaded, since creep compliance curve (Figure 3.5) becomes asymptotic for $t = 40$ *seconds*. Also, for $t > 40$ *seconds* nearly saturated condition is reached by the polymer. On the other hand, response at interphase and fiber are insensitive to loading rates. This is because, the elastic fiber is away from the viscoelastic polymer, whose property changes are relatively drastic.

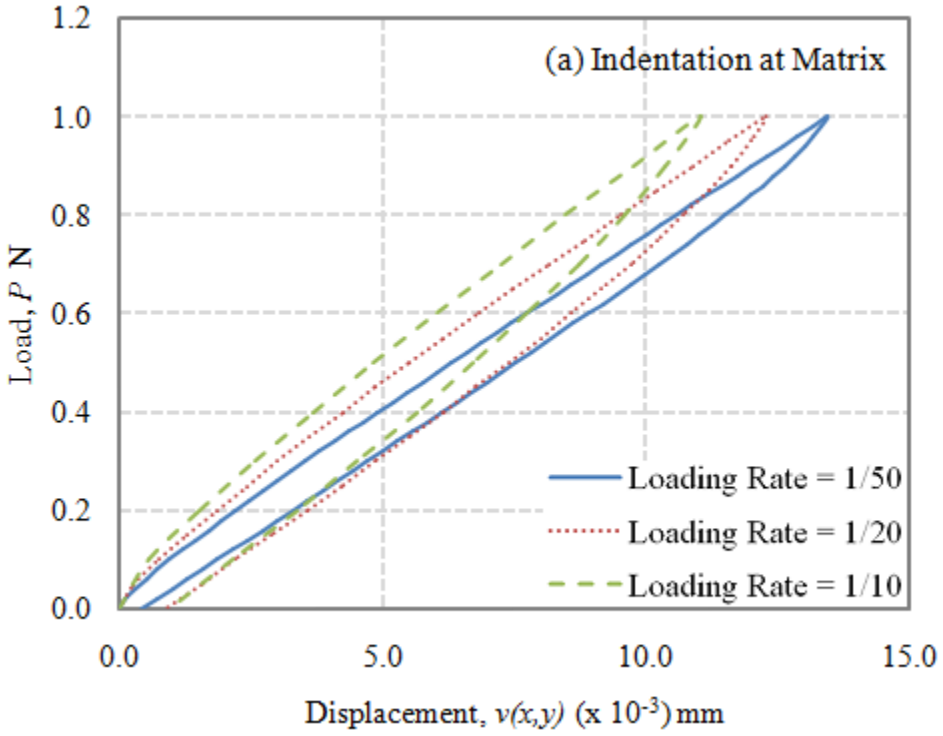

Figure 3.6. Effect of loading rates for indentation at (a) matrix (b) interphase, $E_i/E_0 = 1$ (c) fibre, $E_f/E_0 = 2$, with moisture diffusion.

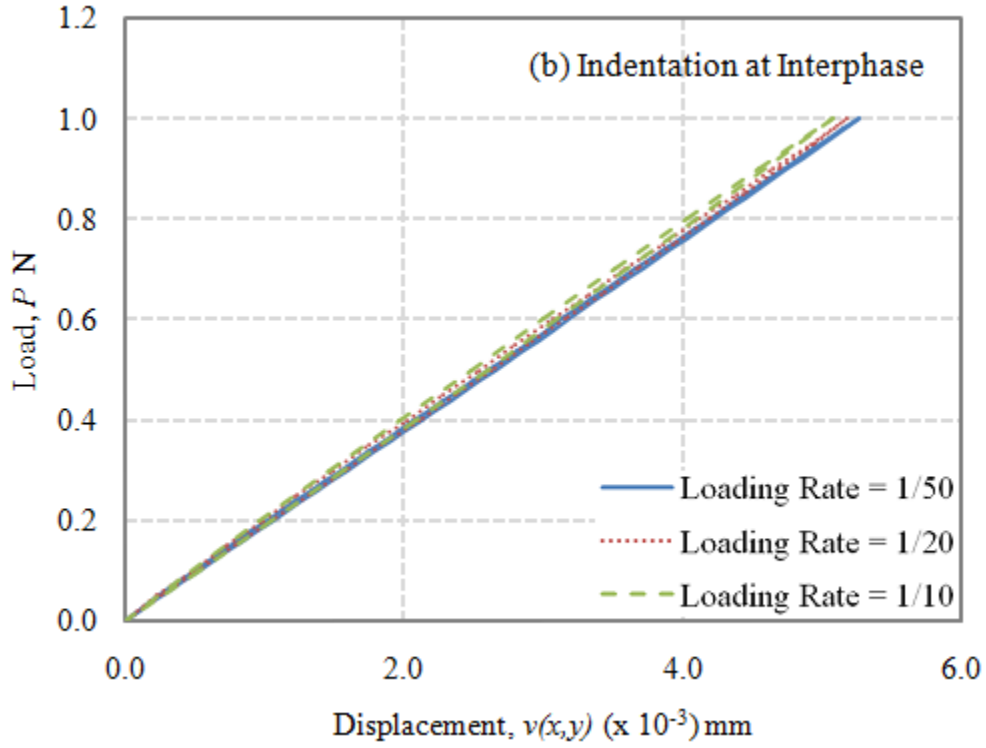

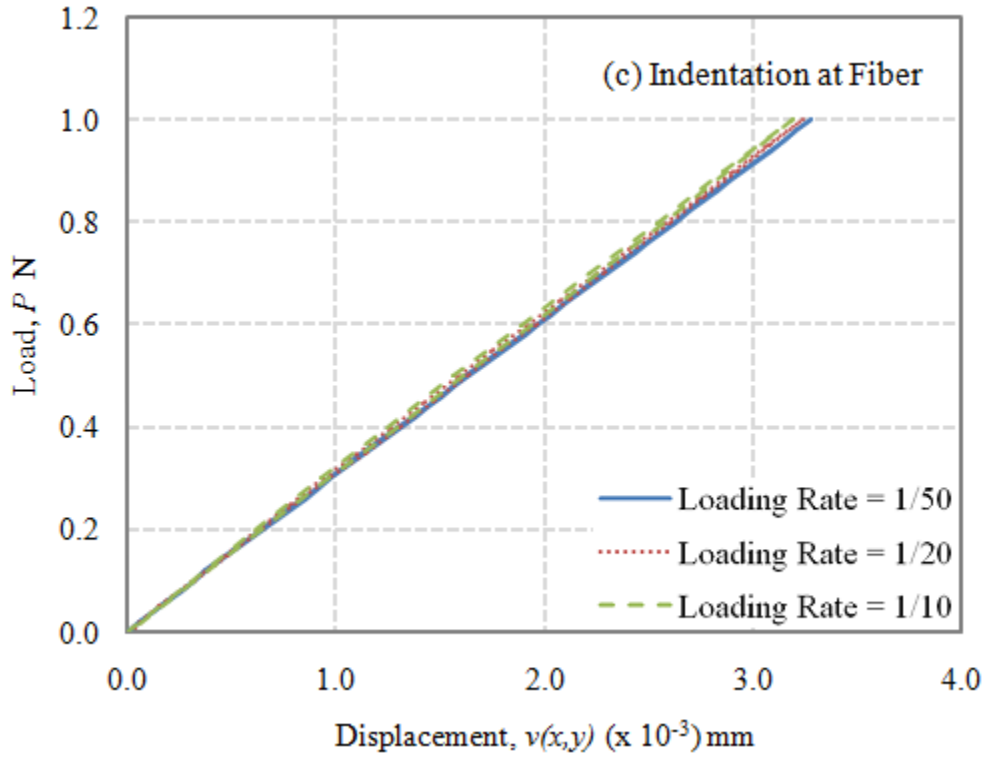

Figure 3.6. cont.

Table 3.3. Average slope (α_{avg}) under the load-displacement curves for indentation at the interphase ($E_f/E_0 = 2,\ E_i/E_0 = 1$) with a viscoelastic matrix and moisture diffusion.

Loading Rate	$\alpha_{avg} \times 10^3$
1/50	0.190
1/20	0.193
1/10	0.197

Table 3.4. Average slope (α_{avg}) under the load-displacement curves for indentation at the fiber ($E_f/E_0 = 2,\ E_i/E_0 = 1$) with a viscoelastic matrix and moisture diffusion.

Loading Rate	$\alpha_{avg} \times 10^3$
1/50	0.305
1/20	0.309
1/10	0.314

Average slope (α_{avg}) is tabulated for each of the loading rates as done earlier. Tables 3.3 and 3.4 for indentation at interphase and fiber respectively are compared with α for elastic matrix ($E_f/E_m = 2,\ E_i/E_m = 1$) from Table 2.3 and Table 2.5. $\alpha_{Em}/(\alpha_{avg})_{Vm}$ is 1.09 for the interphase and 1.04 for the fiber, when the loading is faster (1/10). The observed differences in displacements range from 4-13% for the loading rates simulated, evolution of concentration, assumed forms for creep compliance and degradation of material moduli. In constrast, the corresponding displacements differed by approximately 0.9% for the case of viscoelastic matrix in the dry condition.

C. Effect of indenter tip on the localized response

Point load represents an idealization of indentation. In actuality, there exists a surface contact. In order to study the effect of indenter tips, the case of loading at the softer polymer matrix in the presence of moisture diffusion is considered. Indenters of different shapes and sizes can be used like the ones with pyramidal, cylindrical, spherical and conical tips as shown in Figure 3.8.

In this study, indenter tips of spherical and conical geometries as shown in Figure 3.7 are employed to understand the effect due to a surface contact rather than a point, which is impractical. Surface area of contact between the indenter and the substrate depends both on the shape of indenter as well as the mechanical response of substrate being indented. Based on these factors, the indenter can either push out the displaced material to its sides or push the displaced material further ahead of the indenter. In the former case, contact area increases and is referred to pile-up. The latter effect is called sink-in resulting in a reduced contact area at a given depth [35]. Spherical tip is more likely to cause a pile-up effect, while sink-in effect might be seen in conical tips. In addtion, mechanical response of the material plays an important role in causing these phenomena. Pile-up and sink-in effects are important if one does calculations involving surface area of contact between the indenter and the substrate. The indenters are modeled such that the substrate material do not cross the rigid surfaces of indenters and a rough surface contact is assumed between indenter and substrate. The results and discussion shall now follow:

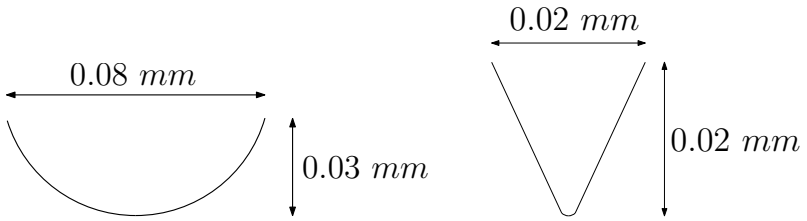

(a) Spherical tip. (b) Conical tip.

Figure 3.7. Indenter tip geometries.

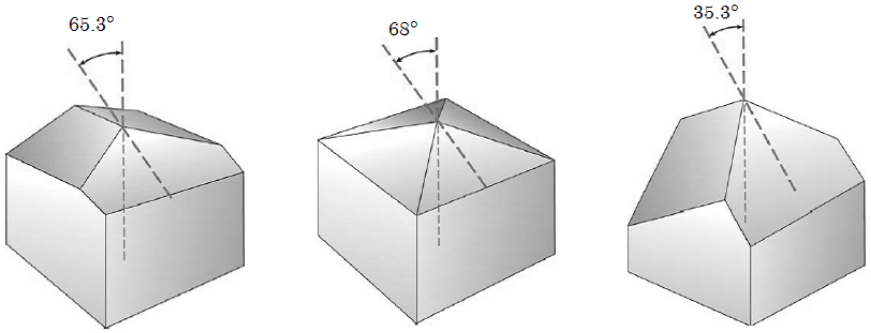

(a) Berkovich (Tip radius: 20-150 nm)

(b) Vickers

(c) Cube-corner (Tip radius: 20 nm)

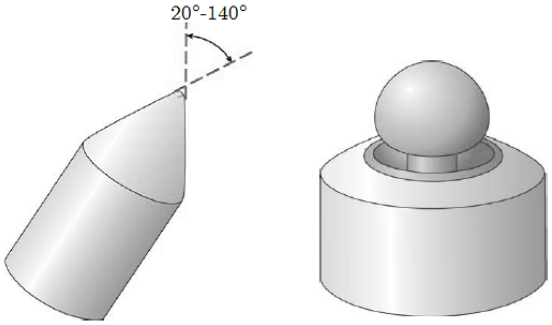

(d) Conical (Tip radius: 20-1000 nm)

(e) Spherical (Tip radius: 150-2000 μm)

Figure 3.8. Common indenter tips in use[7].

[7]Courtesy: Agilent Technologies `http://www.agilent.com`.

A comparison is made in Figure 3.9, of indentation responses with effects of concentration for a loading rate of 1/20. This choice of loading rate is attributed to significant changes in concentration and hence the material properties, at early times. It is observed that different responses are obtained with the indenter tips when compared to the point load. The peak load and its corresponding displacements resulting from the use of indenter tips vary significantly. This is because of the increasing surface area of contact from point load through conical tip to spherical tip. The existence of a surface contact is bound to introduce differences in responses at the fiber and interphase regions as well. Based on the stiffness studies undertaken earlier with a point load, one can only expect slight variations in the fiber and interphase responses with the use of a particular indenter.

Factors influencing the variation of field variables, for indentation with concentration effects include material properties, geometry, loading rate and the surface area of contact of the indenter tip. Changes in distribution of field variables are expected if one alters any of the aforementioned factors, such as, difussivity of the constituents which may increase or reduce the steady state time, Prony coefficients and the retardation times which influence the long time value of the creep compliance, assumed form for shift function that controls the rate of creep, surface area and depth of the indenter tips in contact with the substrate at a particular load and time.

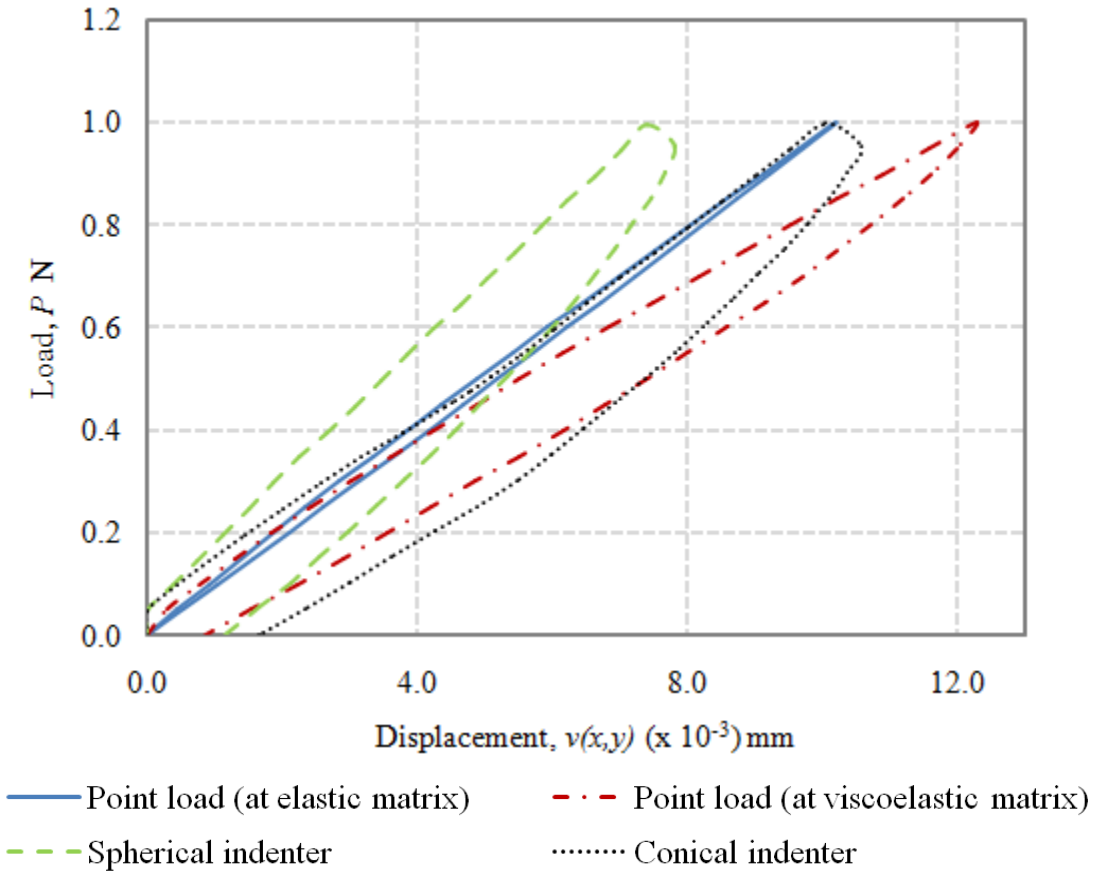

Figure 3.9. Indentation at viscoelastic matrix with moisture diffusion for a loading rate of 1/20, showing the effect of different indenter tips.

From Figures 3.10 and 3.11, although displacement and stress profiles look similar, variations in $|\mathbf{u}|_{max}$ and $(T_v)_{max}$ are observed. Indenter tips result in greater displacement when compared to the point load. Displacements due to spherical and conical tips are comparbale although the latter produces a greater displacement owing to sink-in phenomenon. Stresses due to concentrated load are higher followed by conical tip and least in the case of spherical tip.

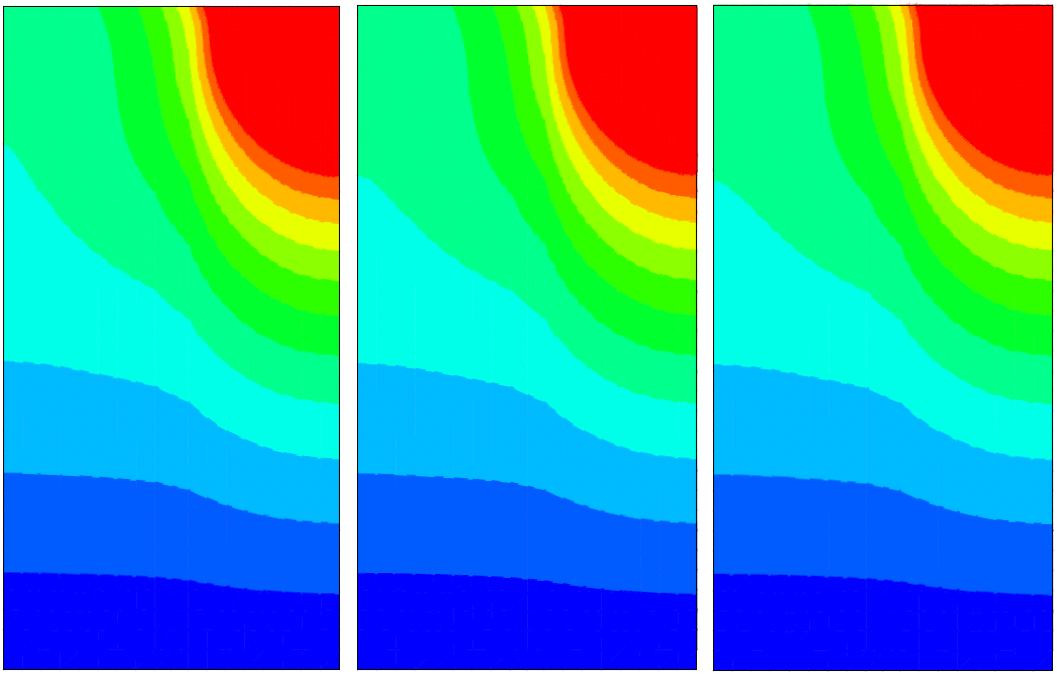

(a) Displacement plot for point load, $|\mathbf{u}|_{max} = 12.298 \times 10^{-3}$ mm.

(b) Displacement plot for spherical indenter, $|\mathbf{u}|_{max} = 27.81 \times 10^{-3}$ mm.

(c) Displacement plot for conical indenter, $|\mathbf{u}|_{max} = 30.57 \times 10^{-3}$ mm.

Figure 3.10. Contour plots for indentation at the viscoelastic matrix ($E_f/E_0 = 2$, $E_i/E_0 = 1$) with moisture diffusion at maximum load (Loading Rate = 1/20), showing displacement variations for (a) point load (b) spherical indenter (c) conical indenter.

Significant differences in responses are observed with respect to the use of different indenter tips. If the observed responses were to change slightly, determination of material properties of heterogeneous media from indentation would be simpler.

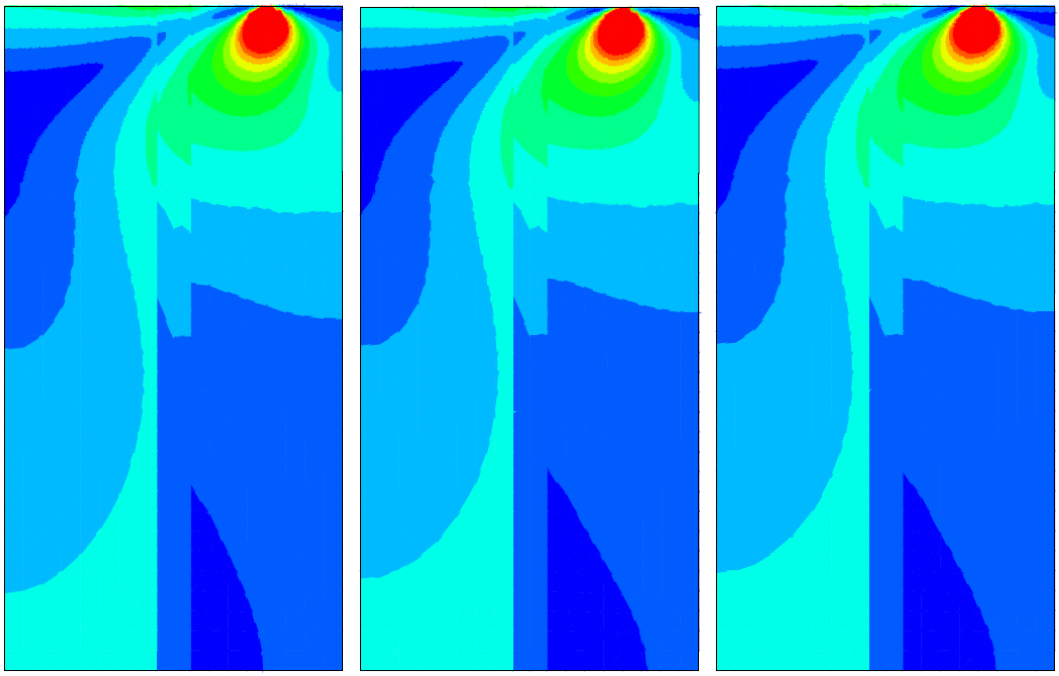

(a) Stress plot for point load, $(T_v)_{max} = 522.127\ MPa$.

(b) Stress plot for spherical indenter, $(T_v)_{max} = 51.38\ MPa$.

(c) Stress plot for conical indenter, $(T_v)_{max} = 234.3\ MPa$.

Figure 3.11. Contour plots for indentation at the viscoelastic matrix ($E_f/E_0 = 2$, $E_i/E_0 = 1$) with moisture diffusion at maximum load (Loading Rate = 1/20), showing stress variations for (a) point load (b) spherical indenter (c) conical indenter.

CHAPTER IV

CONCLUSION AND FUTURE WORK

A. Conclusion

Indentation response of constituents of a FRP composite is numerically simulated using FE. Mechanical characterization of the constituents of a heterogeneous material such as a FRP composite using indentation testing requires, that one understands the localized responses while indenting each constituent as well as the influence of the surrounding constituents on this localized response. Though, the extracted data still needs to be compared with relevant experiments for validation purposes, it provides those first steps towards understanding the material behaviour, when subjected to indentation and simultaneous application of a non-mechanical stimulus like heat conduction or moisture diffusion. Based on the simulations, the following conclusions can be arrived at.

(a) The difficulty in characterizing matrix properties with stiffer surrounding constituents.

(b) The potential of indentation technique to determine interphase properties, if the intricacies involved in indenting the small interphase region can be subdued. This potential can certainly be exploited with advances in instrumentation.

(c) The possibility of determining bond strength of the matrix-fiber interphase.

(d) Fiber properties could be determined from the FE load-displacement data, provided the experimental load-displacement data for indentation at the fiber is made available.

(e) In the presence of a viscoelastic matrix, the surrounding elastic constituents can be characterized by indentation for fast loading rates i.e., when the viscoelastic effects are inconspicuous. With slower loading rates, the viscoelastic effects become prominent making it unfeasible to characterize fiber and interphase properties.

Analytical solutions such as *Flamant* solution which are derived for specific and simplified boundary conditions are inadequate for back calculating fiber properties in heterogeneous materials. Most analytical solutions derived for homogeneous materials assume infinite medium, while in heterogeneous materials, the infinite medium condition with respect to indentation is seldom met entailing a need for numerical solution.

Considering the effects of moisture concentration on the elastic constituents, when the elastic moduli of the constituents were degraded to half their original value, the diplacements increased twofold in the saturated condition as compared to the dry state. When moisture concentration effects are considered along with viscoelastic matrix, greater differences in displacements are observed due to the combined effects of the concentration of fluid and creep, as expected. The use of indenter tips results in varying responses. Infact, the responses due to spherical and conical indenters tips differ considerably, with conical tip producing a greater displacement and concentrated force resulting in greater stresses.

B. Scope for further work

Parametric studies including the effect of Poisson's ratio could be undertaken. Incorporating swelling of the polymer matrix due to moisture absorption and its effect on the indentation response would mean a rigorous analysis. Modeling non-Fickian moisture diffusion simulates realistic conditions. More heterogeneity introduced in

the form of multiple fibers of different sizes with random distribution could be studied. Lastly, FE analysis on a three dimensional model for the FRP composite with real indenter geometries would provide greater insight.

REFERENCES

[1] A. Boersma, V.A. Soloukhin, J.C.M. Brokken-Zijp, and G. De With, "Load and depth sensing indentation as a tool to monitor a gradient in the mechanical properties across a polymer coating: A study of physical and chemical aging effects," *Journal of Polymer Science Part B: Polymer Physics*, vol. 42, no. 9, pp. 1628–1639, 2004.

[2] X. Chen, J. Yan, and A.M. Karlsson, "On the determination of residual stress and mechanical properties by indentation," *Materials Science and Engineering: A*, vol. 416, no. 1-2, pp. 139–149, 2006.

[3] J.J. Vlassak and W.D. Nix, "Measuring the elastic properties of anisotropic materials by means of indentation experiments," *Journal of the Mechanics and Physics of Solids*, vol. 42, no. 8, pp. 1223–1245, 1994.

[4] A.K. Bhattacharya and W.D. Nix, "Finite element analysis of cone indentation," *International Journal of Solids and Structures*, vol. 27, no. 8, pp. 1047–1058, 1991.

[5] H. Lu, B. Wang, J. Ma, G. Huang, and H. Viswanathan, "Measurement of creep compliance of solid polymers by nanoindentation," *Mechanics of Time-Dependent Materials*, vol. 7, no. 3, pp. 189–207, 2003.

[6] G.M. Odegard, T.S. Gates, and H.M. Herring, "Characterization of viscoelastic properties of polymeric materials through nanoindentation," *Experimental Mechanics*, vol. 45, no. 2, pp. 130–136, 2005.

[7] P.L. Larsson and S. Carlsson, "On microindentation of viscoelastic polymers," *Polymer Testing*, vol. 17, no. 1, pp. 49–75, 1998.

[8] S. Laurenzi, T. Albrizio, and M. Marchetti, "Modeling of moisture diffusion in carbon braided composites," *International Journal of Aerospace Engineering*, vol. 2008, Article ID 294681, pp. 1–10, 2008.

[9] J.R. Willis, "Hertzian contact of anisotropic bodies," *Journal of the Mechanics and Physics of Solids*, vol. 14, no. 3, pp. 163–176, 1966.

[10] I.N. Sneddon, "The relation between load and penetration in the axisymmetric Boussinesq problem for a punch of arbitrary profile," *International Journal of Engineering Science*, vol. 3, no. 1, pp. 47–57, 1965.

[11] A.E. Giannakopoulos and S. Suresh, "Indentation of solids with gradients in elastic properties: Part I. Point force," *International Journal of Solids and Structures*, vol. 34, no. 19, pp. 2357–2392, 1997.

[12] T.A. Laursen and J.C. Simo, "A study of the mechanics of microindentation using finite elements," *Journal of Materials Research*, vol. 7, no. 3, pp. 618–626, 1992.

[13] B. Taljat, T. Zacharia, and F.M. Haggag, "Analysis of ball-indentation load-depth data: Part I. Determining elastic modulus," *Journal of Materials Research*, vol. 12, no. 4, pp. 965–974, 1997.

[14] K. Sadeghipour, W. Chen, and G. Baran, "Spherical micro-indentation process of polymer-based materials: A finite element study," *Journal of Physics D: Applied Physics*, vol. 27, pp. 1300–1310, 1994.

[15] G. Care and A.C. Fischer-Cripps, "Elastic-plastic indentation stress fields using the finite-element method," *Journal of Materials Science*, vol. 32, no. 21, pp. 5653–5659, 1997.

[16] S.D. Mesarovic and N.A. Fleck, "Spherical indentation of elastic-plastic solids," *Proceedings: Mathematical, Physical and Engineering Sciences*, vol. 455, no. 1987, pp. 2707–2728, 1999.

[17] E.R. Kral, K. Komvopoulos, and D.B. Bogy, "Elastic-plastic finite element analysis of repeated indentation of a half-space by a rigid sphere," *ASME Journal of Applied Mechanics*, vol. 60, pp. 829–841, 1993.

[18] J.D. Clayton, "Spherical indentation in elastoplastic materials: Modeling and simulation," Tech. Rep., Aberdeen Proving Ground, MD: Army Research Laboratory, 2005.

[19] Y.L. Shen and Y.L. Guo, "Indentation modelling of heterogeneous materials," *Modelling and Simulation in Materials Science and Engineering*, vol. 9, pp. 391–398, 2001.

[20] L. Gan and B. Ben-Nissan, "The effects of mechanical properties of thin films on nano-indentation data: Finite element analysis," *Computational Materials Science*, vol. 8, no. 3, pp. 273–281, 1997.

[21] J.A. Knapp, D.M. Follstaedt, S.M. Myers, J.C. Barbour, and T.A. Friedmann, "Finite-element modeling of nanoindentation," *Journal of Applied Physics*, vol. 85, pp. 1460–1474, 1999.

[22] M. Zidi, L. Carpentier, A. Chateauminois, and F. Sidoroff, "Quantitative analysis of the micro-indentation behaviour of fibre-reinforced composites: Development and validation of an analytical model," *Composites Science and Technology*, vol. 60, no. 3, pp. 429–438, 2000.

[23] M. Desaeger and I. Verpoest, "On the use of the micro-indentation test technique

to measure the interfacial shear strength of fibre-reinforced polymer composites," *Composites Science and Technology*, vol. 48, no. 1-4, pp. 215–226, 1993.

[24] H. Ho and L.T. Drzal, "Evaluation of interfacial mechanical properties of fiber reinforced composites using the microindentation method," *Composites Part A: Applied Science and Manufacturing*, vol. 27, no. 10, pp. 961–971, 1996.

[25] M. Sakai, "Time-dependent viscoelastic relation between load and penetration for an axisymmetric indenter," *Philosophical Magazine A*, vol. 82, no. 10, pp. 1841–1849, 2002.

[26] B. Storåkers and P.L. Larsson, "On Brinell and Boussinesq indentation of creeping solids," *Journal of the Mechanics and Physics of Solids*, vol. 42, no. 2, pp. 307–332, 1994.

[27] M.V.R. Kumar and R. Narasimhan, "Analysis of spherical indentation of linear viscoelastic materials," *Current Science*, vol. 87, no. 8, pp. 1088–1095, 2004.

[28] F. Carrillo, S. Gupta, M. Balooch, S.J. Marshall, G.W. Marshall, L. Pruitt, and C.M. Puttlitz, "Nanoindentation of polydimethylsiloxane elastomers: Effect of crosslinking, work of adhesion, and fluid environment on elastic modulus," *Journal of Materials Research*, vol. 20, no. 10, pp. 2820–2830, 2005.

[29] S. Gupta, J. Lin, P. Ashby, and L. Pruitt, "A fiber reinforced poroelastic model of nanoindentation of porcine costal cartilage: A combined experimental and finite element approach," *Journal of the Mechanical Behavior of Biomedical Materials*, vol. 2, no. 4, pp. 326–338, 2009.

[30] FEA ABAQUS, "Version 6.8," Simulia: Dassault Systemes, Providence, RI, 2009.

[31] A.K. Kaw, *Mechanics of Composite Materials*, Boca Raton, FL, CRC Press, 2006.

[32] D.A. Edwards, "Non-Fickian diffusion in thin polymer films," *Journal of Polymer Science Part B: Polymer Physics*, vol. 34, no. 5, pp. 981–997, 1996.

[33] A.S. Wineman and K.R. Rajagopal, *Mechanical Response of Polymers: An Introduction*, New York, Cambridge University Press, 2000.

[34] R.M. Haj-Ali and A.H. Muliana, "Numerical finite element formulation of the Schapery non-linear viscoelastic material model," *International Journal for Numerical Methods in Engineering*, vol. 59, no. 1, pp. 25–45, 2004.

[35] K.W. McElhaney, J.J. Vlassak, and W.D. Nix, "Determination of indenter tip geometry and indentation contact area for depth-sensing indentation experiments," *Journal of Materials Research*, vol. 13, no. 5, pp. 1300–1306, 1998.

[36] J. Mackerle, "Finite element modelling and simulation of indentation testing: A bibliography (1990-2002)," *Engineering Computations*, vol. 21, no. 1, pp. 23–52, 2004 *.

[37] J. Mackerle, "Finite element and boundary element simulations of indentation problems:: A bibliography (1997-2000)," *Finite Elements in Analysis and Design*, vol. 37, no. 10, pp. 811–819, 2001 *.

[38] R.W. Soutas-Little, *Elasticity*, Mineola, NY, Dover Publications, 1999 *.

[39] W. Zhao, "Modeling of ultrasonic processing," M.S. thesis, Massachusetts Institute of Technology, Cambridge, MA, 2005 *.

* Supplementary sources consulted: [36]-[39]

APPENDIX A

This appendix presents convergence studies for the FE mesh and comparison of FE solution with analytical (*Flamant*) solution available for a concentrated normal force on a homogeneous, isotropic and linear elastic half-plane.

A. Convergence

It is necessary that the results from FE analysis satisfy convergence criteria i.e., the results should not change with mesh size. Hence, mesh refinement studies are conducted for point load at the matrix ($E_f/E_m = 2; E_i/E_m = 1/2$) to justify the use of element size (0.0025×0.0025) used in this study. Owing to singularity at the point of application of load, numerical results at nodes in the immediate neigbourhood of the point load are considered as shown in Figure A.1.

It is observed that the load-displacement curves for the mesh sizes 0.0025 and 0.00125 coincide, satisfying convergence. Mesh sizes 0.01 and 0.005 give reasonably accurate displacements as well. However, these meshes still need to be verified for the stresses. Table A.1 shows that the stresses vary appreciably for the first two meshes, while von Mises stress is nearly converged for the last two meshes.

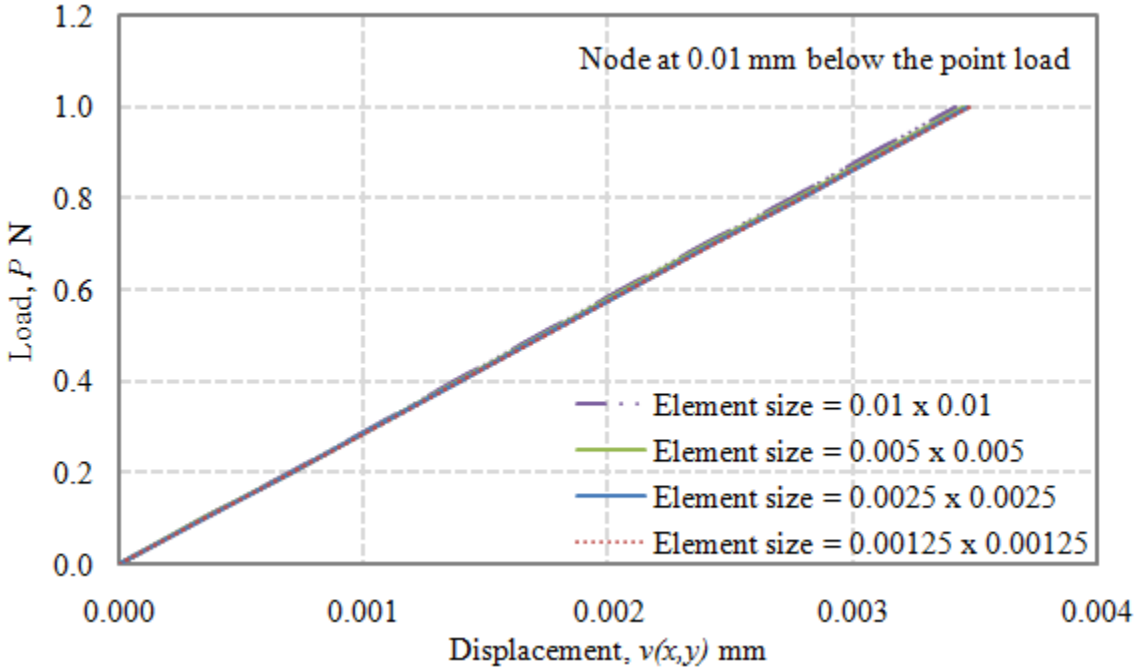

Figure A.1. Displacement, $v(x, y)$ corresponding to the node 0.01 mm below the point load.

Table A.1. von Mises stress, T_v corresponding to the node 0.01 mm below the point load, for different mesh sizes.

von Mises stress, T_v (MPa)				
Load, N	Mesh size: 0.01	Mesh size: 0.005	Mesh size: 0.0025	Mesh size: 0.00125
0.5	33.4586	28.3198	29.2454	29.4978
1.0	66.9173	56.6397	58.4909	58.9957

It is therefore acceptable to use an element size of 0.0025×0.0025.

B. Analytical versus numerical solution

The precision of FE solution is verified by considering the problem of a point load applied on a homogeneous, isotropic and linear elastic half-plane as shown in Figure A.2. Mesh size 0.0025 is used.

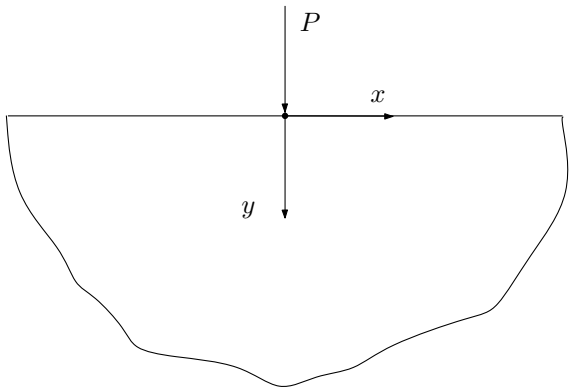

Figure A.2. Point load P acting on the surface of an infinite medium.

Point load P is applied at the origin of the coordinate system. The traction boundary conditions[8] are given by:

$$T_{xy}(x,0) = 0; \quad T_{yy}(x,y) = P\delta(x,y)$$

Near the origin, the concentrated force is like a Dirac delta,

$$\delta(x,y) = 0, \quad x,y \neq 0$$

$$\delta(0,0) \quad \textit{Undefined}$$

[8]Adapted from `en.wikipedia.org`.

The corresponding stresses[9] resulting from the governing equations of elasticity (Plane strain) are:

$$T_{xx} = \frac{2Px^2y}{\pi(x^2+y^2)}; \quad T_{yy} = \frac{2Py^3}{\pi(x^2+y^2)^2}; \; T_{xy} = \frac{2Pxy^2}{\pi(x^2+y^2)^2}; \quad T_{zz} = \nu(T_{xx}+T_{yy}), \tag{A.1}$$

remaining components being zero.

von Mises stress is calculated analytically as:

$$T_v = \left[\frac{3}{2}\, tr(\boldsymbol{\tau}\boldsymbol{\tau}^T)\right]^{1/2}, \tag{A.2}$$

where the deviatoric part of the stress tensor ($\mathbf{T}$) is given by:

$$\boldsymbol{\tau} = \mathbf{T} - p\mathbf{I}, \tag{A.3}$$

p being the mean normal stress.

Since the analytical solution is for an infinite medium and the FE solution is for a finite domain, the effect of increasing the size of the FE domain on the stresses is considered.

Due to singularity at the point of application of load, T_v is computed at locations below the point load. Numerical solution is also obtained by increasing the size of the medium. Figure A.3 shows that the analytical and numerical solutions for von Mises stress are in good agreement albeit there are considerable differences in stresses in the immediate vicinity (upto depth$= 0.0025\ mm$) of point load.

---

[9] Adapted from p.138 of [38].

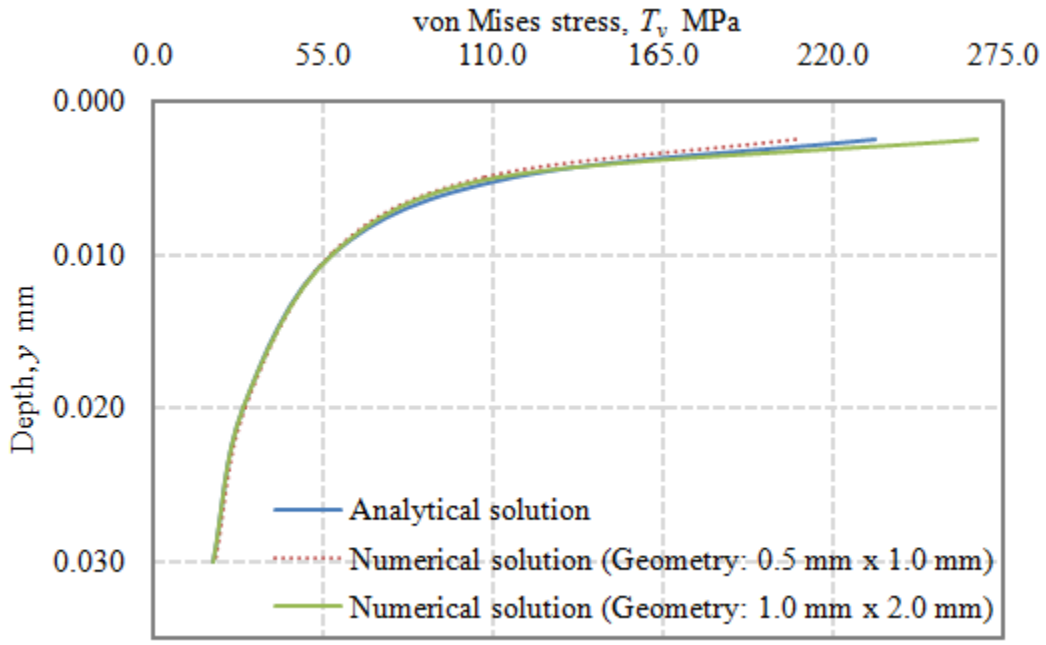

Figure A.3. Comparison of von Mises stress variation.

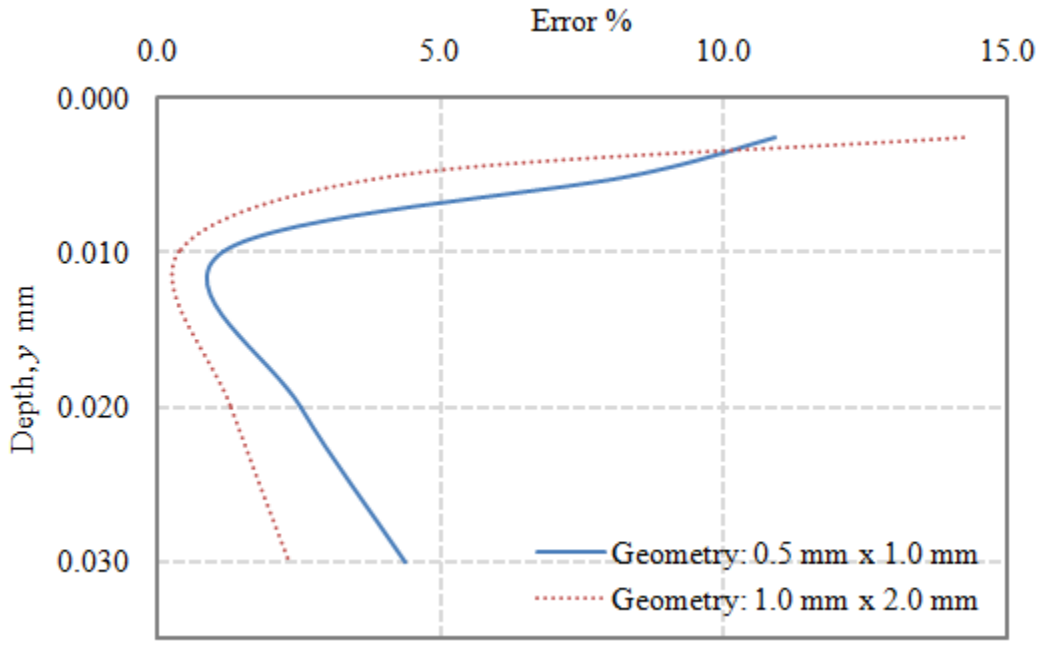

Figure A.4. Variation of error between $(T_v)_{Analytical}$ and $(T_v)_{Numerical}$.

As seen from Figure A.4, error(%) in T_v is higher at locations immediately below (upto depth= 0.0025 mm) the point load. With an increase in medium size, there is a reduction in the error(%). This is because, as medium size increases, numerical solution tends to approach analytical solution (for an infinite medium), which is expected. Considering the vertical component of displacement for the aforestated problem:

$$v(x,y) = -\frac{P(1+\nu)}{\pi E}\left[(1-\nu)\ ln(x^2+y^2) - \frac{y^2}{x^2+y^2}\right]. \tag{A.4}$$

where, P is the force per unit thickness. Numerical solution from ABAQUS for a homogeneous, isotropic elastic solid ($E = 2000\ MPa\ ; \nu = 0.2$) subjected to a point load of magnitude $P = 1\ N$, is compared with that calculated using Equation (A.4)[10]. The error is approximately 4.9% as shown in Figure A.5.

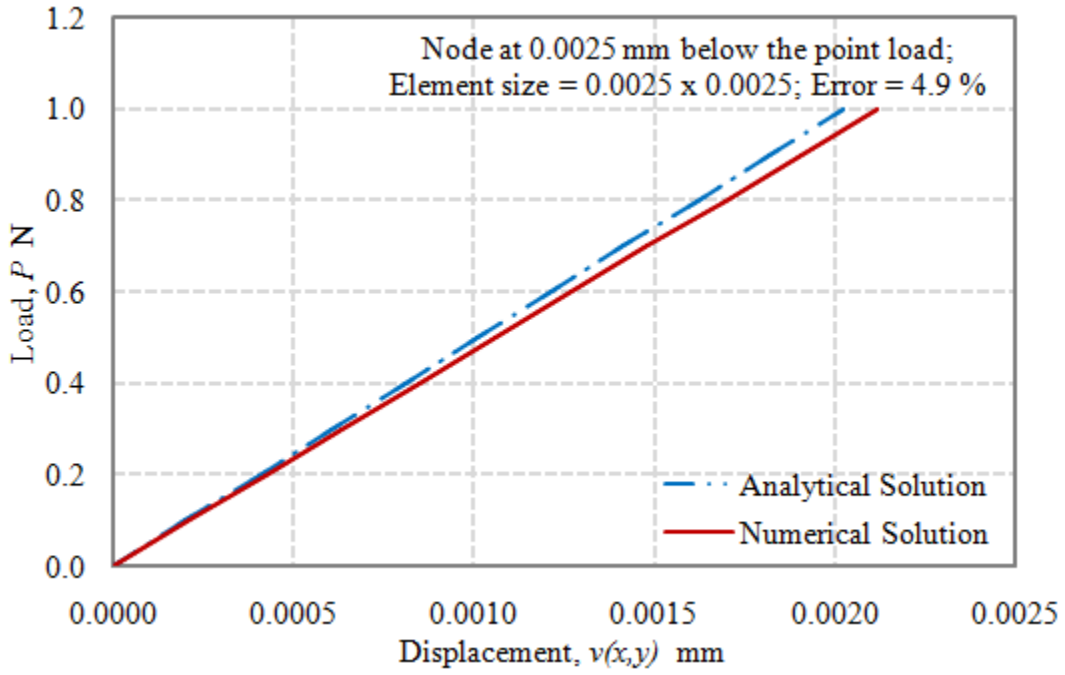

Figure A.5. Comparison of numerical and *Flamant* solutions.

[10]Adapted from p.45 of [39].

With the use of *Flamant* solution, error in von Mises stress and vertical component of displacement are within acceptable limits for a homogeneous medium. But the solution becomes inapplicable for back calculating the properties of individual constituents in a heterogeneous material as evident from Table 2.4 of Chapter II.

VITA

Name: Arun Ravishankar

Address: Department of Mechanical Engineering
c/o Dr. Anastasia Muliana
Texas A&M University
College Station, Texas 77843-3123, USA

Email Address: mecarun@gmail.com

Education: M.S., Mechanical Engineering, 2011
Texas A&M University, College Station, USA

B.E., Mechanical Engineering, 2006
Visvesvaraya Technological University
B.M. Sreenivasiah College of Engineering, Bangalore, India

The typist for this thesis was Arun Ravishankar.